UNITED STATES
DEPARTMENT OF THE INTERIOR
GEOLOGICAL SURVEY

LOW-FLOW TRANSPORT MODELS FOR CONSERVATIVE AND SORBED SOLUTES--

UVAS CREEK, NEAR MORGAN HILL, CALIFORNIA

By Alan P. Jackman, Roy A. Walters and Vance C. Kennedy

Water-Resources Investigation Report 84-4041

Menlo Park, California
1984

UNITED STATES DEPARTMENT OF THE INTERIOR

WILLIAM P. CLARK, Secretary

GEOLOGICAL SURVEY

Dallas L. Peck, Director

For additional information
write to:

Regional Hydrologist, WR
U.S. Geological Survey, WRD
345 Middlefield Road
Menlo Park, California 94025

Copies of this report can
be purchased from:

Open-File Services Section
Western Distribution Branch
U.S. Geological Survey
Box 25425, Federal Center
Denver, Colorado 80225
(Telephone: (303) 234-5888)

CONTENTS

TABLES

ILLUSTRATIONS

LOW-FLOW TRANSPORT MODELS FOR CONSERVATIVE AND SORBED SOLUTES --UVAS CREEK, NEAR MORGAN HILL, CALIFORNIA

By

Alan P. Jackman, Roy A. Walters and Vance C. Kennedy

ABSTRACT

Models describing low-flow solute transport of conservative (nonreactive) species and species which adsorb (react) on the bed are developed and tested. Storage of conservative solutes in the interstitial spaces of the bed plays a significant role in the movement of such species. Three different models of the bed storage process are developed. One model assumes the bed to be a well-mixed, nondiffusing, nonreacting zone. The flux of solute into the bed is then proportional to the difference between stream concentration and bed concentration. A second model assumes that solute in the bed is transported by a vertical diffusion process. The bed concentration, which is the same as the stream concentration at the interface, varies with depth in the bed according to Fick's Law. A third model assumes that the convection in the downstream direction occurs in selected parts of the bed whereas the mechanism of the first model functions everywhere.

Storage of adsorbing species is assumed to occur by equilibrium adsorption occurring at sites within the particles of the streambed sediments. The bed is assumed to consist of particles of a uniform size. The rate of uptake is described by an intraparticle diffusion process.

All model equations were solved using finite element numerical methods. The models were calibrated using data collected at Uvas Creek near Morgan Hill, California. This stream was studied before, during and for 3 weeks following a 24-hour constant-rate injection of conservative chloride ions and

adsorptive strontium ions.

All of the conservative species models are found to very accurately predict observed chloride ion concentrations in the stream. The more elaborate models incorporating bed diffusion and bed convection are found to predict somewhat better.

The adsorption model is found to predict observed strontium ion concentrations well during the injection period but to overestimate somewhat the observed concentrations after the injection ceased. The overestimation may be due to convection of some strontium deep into the bed where it was retained much longer than the 3 week post-injection observation period.

INTRODUCTION

To describe completely the movement of soluble chemical species under low streamflow conditions, transport models for both conservative and nonconservative solutes are needed. Conservative solutes are those whose movement cannot be distinguished from the movement of the water in which they are dissolved. Nonconservative (also termed reactive) solutes are those which are sorbed by the streambed or which chemically react either in solution or on the streambed.

Conservative constituents such as deuterium, tritium, chloride, bromide, and certain organic dyes are often employed during field studies as water tracers. Transport models for conservative solutes permit the determination of the mean hydraulic velocities and residence times in studied reaches as well as dispersion coefficients. They are also useful in determining the extent to which the bed itself serves as a water conveyance.

Most of the solutes of interest, both natural and man-made, are nonconservative. Adsorption of solutes on suspended or bed sediments can be an important factor in controlling the chemical composition of stream waters. This is especially true under low-flow conditions, when the amount of adsorbable solutes in the water column can be small relative to the adsorption capacity of the streambed, as well as under high-flow conditions, when adsorption capacity of suspended sediments may be great due to a high concentration of suspended sediment (Kennedy, 1965). When intermediate flow conditions exist, suspended-sediment concentrations may be moderate to low and quantity of some adsorbable solutes in the water column relatively great compared to the adsorption capacity of the bed; therefore, the effect of stream sediments on water quality will be somewhat less under these conditions.

Because many pollutants are introduced into streams at a relatively constant rate the year around, the concentration of such pollutants will be greatly increased under low-flow conditions and, hence, may be a much greater potential hazard then. This constitutes a strong argument for investigating the uptake of sorbable solutes when streams are at or near low flow. Another advantage of studying streams at low flow is that one can reasonably expect that stream discharge and stream chemistry will change slowly then--as opposed to high-flow conditions--and the logistics of field studies are greatly simplified.

Although there have been a number of theoretical studies made to predict how sorbable solutes might be expected to react with stream sediments, there has been, and continues to be, a shortage of thorough field studies which can be used in testing the various theoretical models or in developing concepts of the major processes controlling sediment-stream interactions.

Developing an understanding of the chemical interaction between stream solids (both inorganic and organic) and associated stream water, as well as developing predictive models for those interactions, is an iterative process. That is, a conceptual model of expected interactions is evolved from available information, field tests are designed and conducted and results are evaluated both qualitatively by scientific reasoning and quantitatively using mathematical models. Either testing procedure can identify errors in the original conceptual model, and the sequence of field testing and reevaluation and refinement of the models can be repeated until satisfactory agreement with field data and observations is achieved.

This study is part of a long-term effort on the part of the U. S. Geological Survey to predict the transport of both conservative and non-conservative solutes in streams in which appreciable physical or chemical interactions with bed, banks, or suspended solids can be expected. Initial work is on small cobble-bed, pool-and-riffle streams because the effect of sediment on water chemistry is expected to be great in such streams, i.e., the reactive capacity of sediment can be large relative to stream discharge. Small streams are preferred to simplify experimental logistics. We anticipate that results of such studies will be helpful in understanding and predicting the important processes not only in small streams but in larger ones as well in which the flow regime and ratio of water volume to wetted stream channel are similar. Processes in large deep rivers or in low-gradient sand-bed streams may be quite different from pool-and-riffle streams in their relative importance in controlling stream chemistry.

The objective of this report is to describe various models of the processes by which conservative and non-conservative solutes are transported by streams when relatively large amounts of such solutes are temporarily stored in the streambed. The conservative solute, chloride, was selected for its lack of sorptive tendencies and the precise analytical methods available. The nonconservative solute, strontium, was selected for its rather simple cation-exchange type interaction with the streambed and its normally low background concentration. The characteristics of cation exchange on streambed sediments are described in detail below, following a description of the experimental site and the 24-hour solute injection. Then several conceptual and mathematical models for conservative solute transport and one model for transport of an adsorbed solute are developed. An Eulerian finite element numerical technique (see Appendix for details) was employed and is briefly

described. The choice of numerical technique is not important to the principal objective of this work, and other techniques (e.g. Lagrangian or finite difference) would be satisfactory also. Finally, the models are evaluated by comparison of model predictions with experimental observations and suggestions for future model improvement are made.

Uvas Creek Experimental Site

The field experiment described here was conducted in Uvas Creek, a small, unpolluted, cobble-bed, pool-and-riffle stream located in west central Santa Clara County, California about 13 km west of the town of Morgan Hill. Factors important in site selection were good accessibility, relatively low dissolved solute concentrations and low biological activity. The study reach (Figure 1) dropped 18.6 m in elevation over a 640 m distance. Stream discharge averaged about 0.022 m^3 sec^{-1} during the 24-hour period of injection.

Most of the bed was composed of gravel and cobbles greater than 4 mm in diameter, although pools contained some finer grained bed materials including some organic sediments. The channel is cut predominantly into unconsolidated sedimentary deposits. The adjoining slopes are generally quite steep and are underlain by folded and faulted, highly lithified sediments. Gravel fills the bottom of the channel but, judging from the shapes of the confining slopes, such deposits are probably quite thin--on the order of a meter or two in depth. There are occasional gravel bars deposited in wider parts of the channel.

The discharge showed a large diurnal variation and was monitored continuously using a Parshal flume at the lower end of the study reach. Discharge was measured at the head of the study reach using a salt-dilution technique. Due to the high stream gradient and the coarse nature of the bed materials, it is likely that there is some flow in the bed. This is particularly likely in

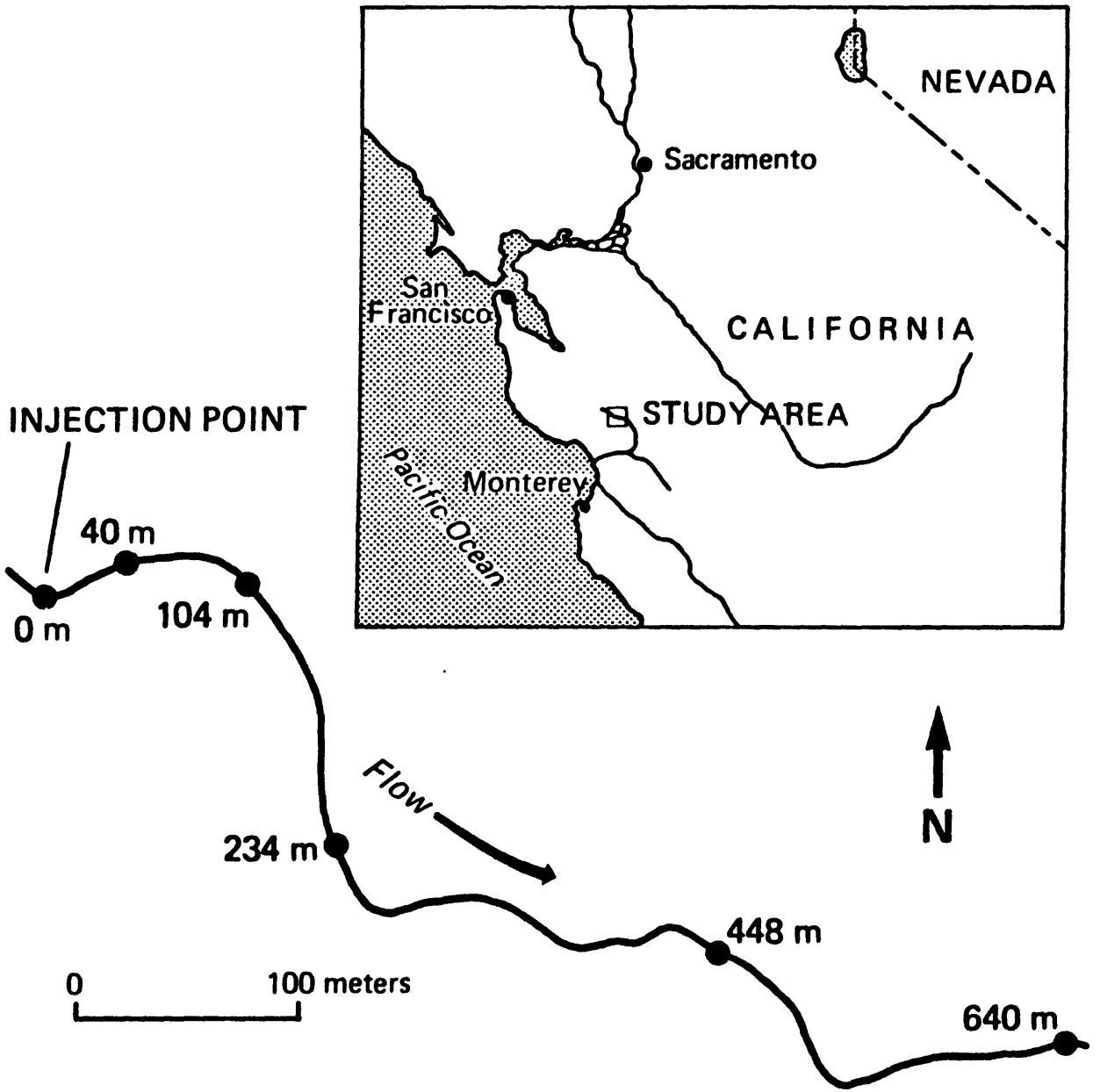

Figure 1. Map of the Uvas Creek study reach showing locations of sampling stations.

the zones underlying the downstream ends of pools. This may be a mechanism by which some of a conservative tracer could be temporarily stored in the bed during the passage of the injected pulse. In the absence of net flow into the bed, diffusion or dispersion of a conservative solute could also store that solute in the water-filled interstices of the bed. Bank storage of solute-laden waters is another possible storage mechanism. But, whereas stage differences of 1-2 cm occurred as a result of diurnal flow variations, it is unlikely that bank storage was the major mechanism owing to the low permeability of the sedimentary banks, the absence of extensive gravel banks, and the fact that ground-water inflow will tend to oppose flow outward into the banks. In the study reach, Uvas Creek is a gaining stream and even during the low-flow period of August and Septemeber, several seeps are visible.

The Field Experiment

The principal experiment involved a constant-rate 24-hour injection of solution containing strontium and chloride ions made at the head of the study reach on September 12-13, 1973. Background water samples were collected for several days prior to the start of the injection, and concentrations of all species were found to be constant and independent of sampling location. All concentrations reported here are net, i.e. the difference between observed concentration and backgkround concentration. During the injection, samples were collected at 5 stations (40, 104, 234, 448 and 640 mm below the injection point, Figure 1) with very frequent sampling during the arrival of the leading edge and the departure of the trailing edge of the high-concentration pulse. Sampling at stations 2-4 continued infrequently for 1 week and at station 5 for 3 weeks after completing the injection. Details of the experimental design are reported elsewhere (Kennedy, et al., in preparation). An earlier

study at this site employing a similar injection of 3-hour duration has been reported by Zand and others (1976).

In addition to discharge and concentration data, a considerable amount of auxiliary chemical and physical data was collected at the experimental site. This included detailed channel geometry (depths, widths, wetted perimeters at transects located approximately every 6 m along the channel. Data on distribution of particle sizes in the bed were also collected at the same transects. A 1:600 scale map of the channel and surroundings was prepared by a field crew from the Topographic Division of the U.S. Geological Survey.

The magnitude of ground water inflow was estimated based on a Cl mass balance assuming Cl to be a conservative tracer. At each station the product of observed concentration and discharge measured at the injection site was integrated over time to give total mass of Cl passing that station. Because of the extended dieaway, it was necessary to extrapolate Cl concentrations by fitting decaying exponential functions to data in the tail of the observed dieaway. Assuming all mass passed station 1, the mass passing each subsequent station was forced to agree with that passing station 1 by increasing flow by a fixed percentage over that observed upstream. Flow increases with respect to station 1 were calculated as 0, 6.4, 8.2 and 11.2 percent for stations 2 through 5 respectively. There is some uncertainty about the value for station 5 because of the difficulty in estimating the large amount of low concentration Cl which continued to discharge for about 3 weeks following the injection.

It is recognized that a significant amount of stream water percolated into the bed and bank gravel deposits only to return later at a downstream point after a considerable time delay. During the period when the tracer-laden water was displacing the original interstitial fluid, the

displaced water entered the stream in a manner which cannot be distinguished from ordinary ground-water inflow. In the case of tracer solution with a residence time longer than the injection period, such return flow can be treated for modelling purposes as though it were indeed ground-water inflow. At this point we do not know what fraction of the inflow from the banks is returning stream water. Thus, much of the so-called ground water inflow in the model may well have been displaced interstitial water. Additional work may help to determine the extent to which true ground-inflow occurred.

To determine the adsorption characteristics of the streambed, an aggregate sample of bed materials was removed from the creek and segregated, according to size (210-250, 420-500, 841-1000, 1680-2000, 3360-4000 mm ranges). Cation-exchange capacity was determined for each size fraction by saturating a sample with 1N strontium chloride and then desorbing with 1N ammonium acetate. In addition, numerous 10 gram samples of each size fraction were placed in porous polyester bags which were set on the streambed below the injection site prior to the start of the injection. These bags were withdrawn periodically after the injection was started, desorbed with 1N ammonium acetate and analyzed for adsorbed Sr. These samples provide data on the rate of adsorption as well as the distribution coefficient under field conditions.

ION EXCHANGE CHARACTERISTICS OF STREAM SEDIMENTS

In modeling solute interactions with the streambed it is important to understand some of the general adsorption characteristics of stream sediments and the reasons for those characteristics. Typically, in areas of moderate to high relief, streambed sediments contain materials ranging widely in grain size, i.e. from clay, through silt and sand to coarse gravel, or even boulders. Although the surficial materials on a streambed may be composed almost entirely of coarse sand, granules and cobbles due to stream scouring, below that armored surface one commonly finds considerable amounts of much finer sediments as interstitial filling material. Such fine sediments may have greater chemical reactivity than the coarse particles making up the bulk of the bed sediment. Therefore, water percolating through streambed sediments may encounter somewhat more sorptive capacity per unit volume below the bed surface than at the surface. Although it is commonly assumed that reactive surface area consistently decreases with grain size of sediments, this is not always the case; the composition as well as grain size affects the sorptive capacity. Not infrequently, there are dual maxima in a plot of cation-exchange capacity (CEC) versus grain size because of the existence of clay and silt (highest CEC) as independent grains in the finest materials, independent grains of quartz, feldspar and various heavier minerals having low CEC in the coarse-silt and fine-sand range, and aggregates of clay and silt forming coarse sand, granules, cobbles and coarser materials displaying moderately high CEC in the larger sizes (Kennedy, 1965). As the clay and silt aggregates increase in size beyond that of coarse sand the fraction of any particle's volume which is in the reactive surface rind becomes smaller, so the CEC per unit weight then tends to decrease with further increase in grain size.

In order to discuss the cation exchange further, we must have a chemical model of the process as a reference. Cation exchange may be viewed as a reversible reaction involving two free cations, $A^{\alpha+}$ and $B^{\beta+}$, where α and β are the respective valences of A and B, and the bound (adsorbed) forms of both cations, denoted $\bar{A}$ and $\bar{B}$. We will assume for purposes of this discussion that all surface sites bind identically although this will not in general be the case. The chemical reaction may be written

$$\alpha\bar{B} + \beta A^{\alpha+} \rightleftarrows \beta\bar{A} + \alpha B^{\beta+} \tag{1}$$

A rigorous thermodynamic equilibrium expression for this reaction may be written as

$$K_{eq} = \frac{a_{\bar{A}}^{\beta}\, a_{B}^{\alpha}}{a_{\bar{B}}^{\alpha}\, a_{A}^{\beta}} \tag{2}$$

where K_{eq} is the equilibrium constant, $a_{\bar{A}}$ and $a_{\bar{B}}$ are the chemical activities of the bound cations and a_A and a_B are the chemical activities of the cations in bulk solution. If we define activity coefficients, $\gamma_{\bar{A}}$, $\gamma_{\bar{B}}$, γ_A, γ_B as

$$\begin{aligned} \gamma_{\bar{A}} &= a_{\bar{A}}/m_{\bar{A}} \\ \gamma_{\bar{B}} &= a_{\bar{B}}/m_{\bar{B}} \\ \gamma_A &= a_A/m_A \\ \gamma_B &= a_B/m_B \end{aligned} \tag{3}$$

where $m_{\bar{A}}$, $m_{\bar{B}}$, m_A and m_B are the respective molalities for the bound species on the solid exchanging substrate and the unbound ions in the bulk solution, then equation 2 may be written

$$K_{eq} = K_{\gamma}\, K_B^{A} \tag{4}$$

where

$$K_{\gamma} = \frac{\gamma_{\bar{A}}^{\beta} \; \gamma_{B}^{\alpha}}{\gamma_{\bar{B}}^{\alpha} \; \gamma_{A}^{\beta}} \tag{5}$$

and

$$K_{B}^{A} = \frac{m_{\bar{A}}^{\beta} \; m_{B}^{\alpha}}{m_{\bar{B}}^{\alpha} \; m^{\beta}} \tag{6}$$

The ratio K^{A}_{B} is generally referred to as the "selectivity coefficient."

The equilibrium constant, K_{eq}, is a true thermodynamic equilibrium constant and as such has the desirable property that it depends only on temperature. The selectivity coefficient, K^{A}_{B}, may depend on pressure, the nature of the solid, the molalities m_A, m_B, $m_{\bar{A}}$ and $m_{\bar{B}}$ and the molalities of other ionic species present in addition to temperature. Thus, if it is to be used to calculate ion-exchange equilibria, its value must be known as a function of all the above variables. Unfortunately, the determination of activity coefficients is, in general, a difficult problem and thermodynamic data for cations adsorbed on clay minerals is not readily available. Therefore, it has been common in the literature to report selectivity coefficients for various cations on clay minerals.

In practice it is often found that selectivity coefficients are nearly independent of solution concentrations over broad ranges of concentration (Reddy and Marinsky, 1971, Reddy, Amdur and Marinsky, 1972). Helfferich (1962) reported that selectivity coefficients usually do exhibit some dependence on temperature. The tendency is for the selectivity coefficient to move

toward unity with increasing temperature because many of the processes which contribute to selectivity result from association phenomena, e.g. complexation, ion-pair formation and solvation, which generally diminish with increasing temperature.

In this study we are interested in describing the rate of uptake of specific cations per unit of bed area by bed sediments at a particular axial position in a stream. This information is needed for the bed flux term, N_b, which appears in the species conservation equation (see Solute Transport Models).

Consider the uptake of adsorbable cations by particles of a given size. As the actual rates of adsorption and desorption are extremely fast in most cases, it is reasonable to assume that the rate of uptake by the particles is diffusion limited and that, at any point within a particle, the intraparticle fluid concentration is in equilibrium with the adsorbed fluid concentration (Helffrich, 1962).

In describing ion-exchange equilibrium of cations present in greatly differing concentrations, the use of the distribution coefficient, K_d, to describe the equilibrium of the low-concentration cation has become common. The distribution coefficient is defined as the ratio of the concentration of the adsorbed cation to the concentration of the cation in solution. We may rearrange equation 6 to obtain an expression for the distribution coefficient,

$$K_{d,A} = \frac{\bar{m}_A}{m_A} = \left[K_B^A \frac{\bar{m}_B^{\alpha}}{m_B^{\alpha}} \right]^{1/\beta} \qquad (7)$$

If A is a trace cation and B is the major cation, then the distribution

coefficient, $K_{d,A}$ will remain virtually constant unless the molality of B in solution, m_B, changes because K^A_B and $m_{\bar{B}}$ will be nearly constant. If solution molality of the major cation, m_B, varies, the logarithm of $K_{d,A}$ will vary linearly with the logarithm of m_B, the slope being $-\alpha/\beta$. Wahlberg and Fishman (1962) observed such dependence on clay minerals, Bunzl et al. (1976) observed such dependence on acid-washed peat and Reddy and Marinsky (1971) observed such dependence on polystyrene-sulfonic acid resins.

Some solutes are believed to be adsorbed by mechanisms other than ion-exchange (Jenne, 1977). In most such cases it has been found that such adsorption follows a Langmuir isotherm

$$\frac{m_{\bar{A}}}{m_A} = K_{d,A} = \frac{m_{\bar{A},max}}{k_A + m_A} \qquad (8)$$

where $m_{\bar{A},\ max}$ is the Langmuir capacity, the maximum adsorbed molality of species A and k_A is the value of m_A at which $m_{\bar{A}} = \frac{1}{2}\, m_{\bar{A},\ max}$.

Both equations 7 and 8 indicate that the distribution coefficient, $K_{d,A}$ can be expected to be nearly constant in circumstances in which, a) species A is a trace constituent and, b) the major cation(s), B, is present in nearly constant concentration. This fact is useful in developing a model for the rate of adsorption by bed sediments.

SOLUTE TRANSPORT MODELS

The three-dimensional, time-averaged conservation equation for a species in a constant density mixture may be written as

$$\frac{\partial C}{\partial t} + \underline{v} \cdot \nabla C = \nabla \cdot D_{eddy} \nabla C + r \qquad (9)$$

where C is the species concentration, $\underline{v}$ is the velocity vector, D_{eddy} is the eddy diffusivity (assuming isotropic turbulence), r is the homogeneous rate of generation of the species per unit volume and ∇ is the gradient operator. In many situations of practical interest in stream modeling, even those where a point source of the species is involved, mixing in the vertical and lateral directions is quite rapid. In such situations, where species concentrations are essentially uniform over the entire cross-section normal to the trend of the thalweg, averaging equation 9 with respect to the width and depth considerably simplifies modeling, reducing the 3-dimensional species conservation equation to a 1-dimensional species conservation equation

$$A \frac{\partial C}{\partial t} + vA \frac{\partial C}{\partial x} = \frac{\partial}{\partial x}(AD \frac{\partial C}{\partial x}) - \frac{AN_b}{d} \qquad (10)$$

where A is the cross-sectional area, C is the area-averaged species concentration, v is the area-averaged axial velocity, D is the dispersion coefficient, d is the average depth and N_b is the flux of the species from the stream into the bed (Harleman, 1971). Velocity is calculated as $v = Q/A$.

The bed flux term arises from the boundary conditions when integrating equation 9 over the cross-sectional area. It may be thought of as a

source/sink term for solute in the stream. This term couples the stream model of equation 10 to a bed storage model. There are a number of bed storage processes which could contribute to this term, such as diffusion into the interstitial fluid in the bed, lateral fluid traps and adsorption onto the bed materials themselves. Several different models will be discussed below. These models differ not only in the mathematical representation of the bed flux term but also in the physical processes which are described by the various mathematical representations. For the purpose of this development, the mass generation term has been dropped as none of the species injected at Uvas Creek are believed to appear or disappear as a result of reaction in the bulk fluid.

Material entering the bed by any process has left the main channel and must be accounted for. Most material entering the bed can be expected to return, ultimately, to the channel. Therefore, we may think of material being "stored" in the bed. In the case of the species injected at Uvas Creek, we assume that the Cl does not bind to the bed material and all Cl stored in the bed is returned to the main channel. Sr is known to adsorb on clay minerals. It is possible that some of the adsorbed Sr may be permanently bound ("fixed") by the bed. However, there is no indication of fixation in either the laboratory or bag-sample analyses. We will assume, therefore, that all adsorbed Sr is ultimately returned to the channel.

Integrating the product of the discharge and the species concentration observed at a station with respect to time gives an estimate of the mass of a species leaving that station.

As explained above, discharge observed at the upstream end of the reach was adjusted upward a fixed percentage at each downstream station to force the total mass of Cl passing each station to equal the mass of Cl injected. This

assumes that Cl stored in the bed is returned to the channel rather rapidly.

A similar mass balance for Sr using adjusted discharges reveals that 30-40 percent of the injected mass remained in storage 3 weeks after the injection ceased. Much of this storage occurred in the reach between stations 4 and 5. Assuming that fixation was not occurring, it seems probable that most of this storage occurred as a result of flow entering the bed and returning to the channel just downstream. Such a process, somewhat analogous to the retardation of a pulse of adsorbable material passing through a chromatographic column, would permit these strongly adsorbed species to be retained for weeks in a bed zone having a very short hydraulic residence time.

With this background, let us look at several possible physical concepts of the bed storage process and the mathematical models used to represent them.

Exchange Model

This model uses the mass transfer coefficient formulation, mathematically similar to a first order reaction rate expression, for the bed flux

$$N_b = k_g(C-C_b) \tag{11}$$

where k_g(m/sec) is the "mass-transfer coefficient" (see Bird and others, 1960) and C_b is the concentration in the bed. This model is most appropriate to transport between two well-mixed phases where film transport at the phase interface is the rate-limiting process. Thus, we envision the bed as a well-mixed compartment of finite depth underlying the stream. Assuming that no flow or dispersion occurs in the bed, we may model the bed concentration as

$$A_{ex}\frac{\partial C_b}{\partial t} = \frac{A_{ex}}{d_b}N_b$$

$$C_b=0 \quad \text{at} \quad t=0 \tag{12}$$

where A_{ex} is the cross-sectional area of the bed and d_b is the depth of the bed. The form of equation 12 is similar to that of equation 10 with the convective and dispersive terms deleted. The sign of the bed flux term must also be reversed to account for the fact that N_b is positive for movement out of the described channel and since N_b is positive for material flowing from stream to bed, $-N_b$ will be the appropriate flux from bed to stream.

Equations 10, 11 and 12 constitute a complete model of the streambed system. As the interfacial area for transport from the main channel must equal the interfacial area for transfer into the bed, the known width of the main channel, A/d, must equal the width of the bed A_{ex}. Thus there are only two free parameters associated with the storage process for this model, A_{ex} and k_g.

Diffusion Model

This model assumes that solute enters the bed by a dispersive process in the vertical direction. The flux of material into the bed may be described by a Fickian diffusive relationship

$$N_b = -D_b \frac{\partial C}{\partial z}\bigg|_{z=0} \tag{13}$$

where D_b is the bed diffusivity and z is measured in the direction normal to the stream-bed interface. At the interface z = 0 and z increases with increasing depth in the bed.

For this model the bed cannot be assumed to be well mixed. Instead, the species conservation equation must be solved in the z direction. We will assume no convective or diffusive fluxes in the axial (x) or transverse (y) directions. Further, as was the case with the exchange model, we assume that the bed has the same width as the stream channel and is of finite depth, d_b.

Thus the bed concentration is given by

$$\frac{\partial C_b}{\partial t} = D_b \frac{\partial^2 C_b}{\partial z^2} \qquad (14)$$

$$C_b = 0 \quad \text{at} \quad t = 0$$

$$C_b = C \quad \text{at} \quad z = 0$$

$$\frac{\partial C_b}{\partial z} = 0 \quad \text{at} \quad z = d_b$$

Here we assume that the concentration at the streambed interface is the bulk stream concentration and that the bottom of the bed at $z = d_b$ is impervious to the flow of mass.

Equation 14 also resembles equation 10 but without the convective and bed flux terms. Unlike the exchange model, equation 14 specifies that the vertical concentration distribution is needed to calculate bed flux using equation 13.

Like the exchange model, the diffusion model contains two free parameters which describe the storage process. If we assume that diffusion occurs only into the bed immediately below the stream, we are free only to adjust d_b and D_b.

Underflow Model

The underflow model assumes the existence of a flow channel underlying the streambed interface. Streamflow enters this channel through the bed at one location and returns to the stream via the bed at another. Thus, a convective flux describes movement of material into and out of the bed. Because it is very difficult to assess the location of such channels, the model reported here employed only one. This required that some other model be used to describe the storage throughout the rest of the bed. The exchange

model was selected for this purpose. Flow into and out of the underflow channel was treated as an advection. At the point of inflow, the main channel discharge Q was reduced by the amount of the underflow Q_u. As the material entering the underflow channel must have a composition identical to the bulk stream at that point, the stream composition is unaffected. At the point of return, the main channel discharge must again be increased and the concentration in the channel must be adjusted to account for the mixing of the underflow with the main flow. The concentration change in the main channel resulting from this mixing process is given by

$$C'' = \frac{Q'C' + Q_u C_u}{Q' + Q_u} \tag{15}$$

where C' and C" are the main channel concentrations just upstream and downstream of the point of mixing respectively, C_u is the concentration of the returning underflow and Q' is the main channel discharge just upstream of the point of return. The composition in the underflow channel is described by the convective-dispersion equation with no flux term

$$A_u \frac{\partial C_u}{\partial t} + Q_u \frac{\partial C_u}{\partial w} = A_u D_u \frac{\partial^2 C_u}{\partial w^2} \tag{16}$$

$$C_u = 0 \quad \text{at} \quad t=0$$
$$C_u = C \quad \text{at} \quad w=0$$
$$\frac{\partial C_u}{\partial w} = 0 \quad \text{at} \quad w=L_u$$

where A_u is the cross-sectional area of the underflow channel, D_u is the dispersion coefficient for the underflow channel and L_u is the length of the

underflow channel.

The underflow process adds 4 additional free parameters to the two which occur in the exchange model--A_u, L_u, D_u and Q_u. The large number of free parameters here poses some serious problems which will be discussed below.

Adsorption Model

The adsorption process requires a considerably more complex model than those discussed above. The rate of movement of an adsorbable species may be limited by either the rate of diffusion into the bed or the rate of diffusion into the particles composing the bed or both. If both processes affect the rate, convective-dispersion problems in three different directions--axially in the main channel, vertically in the bed and radially in the particles--must be solved. To reduce the complexity of the model, two simplifying assumptions will be made. First, we assume that the concentration of the adsorbable species surrounding all the particles is independent of depth in the bed. And second, we will assume that the particles have planar geometry. Aris (1965) has shown that in the case of diffusion-limited reaction in catalyst pellets, the choice of geometry has little effect on calculation of reaction rate. Helffrich (1962) found that local adsorption rates are much greater than the rates at which adsorbate can diffuse to sites for adsorption, even in material of small particle size. Therefore, we will assume that at any position in the particle, the adsorbate in solution in the pore fluid is in local equilibrium with that adsorbed on the adjacent solid phase. If we further assume that the adsorbate is not the major adsorbable species, the distribution coefficient, K_d, may be assumed to be constant as discussed in Ion Exchange Characteristics of Stream Sediments and we may write

$$n = K_d \tilde{C} \tag{17}$$

Where n is the local adsorbed concentration (mass of adsorbate/mass of adsorbent) and $\tilde{C}$ is the local mass concentration of solute in the pore fluid.

The species continuity equation describing the concentration of adsorbate as a function of position, z, within a flat particle is

$$\varepsilon_p \frac{\partial \tilde{C}}{\partial t} = D_e \frac{\partial^2 \tilde{C}}{\partial z^2} + r \tag{18}$$

where $\tilde{C}$ is the intraparticle concentration, ε_p is the particle void fraction (porosity), D_e is the effective diffusivity and r is the local volumetric rate of production of adsorbate in the pore fluid. The production term must account for the loss or gain of soluble adsorbate in the pore fluid due to adsorption or desorption respectively from the adjacent solid surfaces. As mass accumulating on the solid surface per unit of total particle volume is the negative of the production rate in equation 18, we can express that rate as

$$r = -\rho_p \frac{\partial n}{\partial t} \tag{19}$$

and replacing n in equation 19 with equation 17,

$$r = -\rho_p K_d \frac{\partial \tilde{C}}{\partial t} \tag{20}$$

where ρ_p is the particle density. A complete description of the concentration profile within a flat particle of half-thickness L_p may now be written as

$$(\varepsilon_p + \rho_p K_d) \frac{\partial \tilde{C}}{\partial t} = D_e \frac{\partial^2 \tilde{C}}{\partial z^2} \tag{21}$$

$$\tilde{C} = C \quad \text{at} \quad z=0$$

$$\frac{\partial \tilde{C}}{\partial z} = 0 \quad \text{at} \quad z=L_p$$

$$\tilde{C} = 0 \quad \text{at} \quad t=0$$

Note that the equilibrium adsorption has reduced equation 18 to a simple diffusion equation. The boundary conditions here assume that the adsorbate concentration at the surface of the particle is equal to the stream concentration and that the pore concentration profile is symetrical about the mid-plane of the particle. In all calculations we neglected ε_p as small with respect to $\rho_p K_d$.

The solution to equation 21 will now permit the calculation of the bed flux term in equation 10. The flux of adsorbate into the particle is given by

$$-D_e \frac{\partial C}{\partial z}\bigg|_{z=0}$$

Thus the volumetric uptake rate for a single particle, r_p, may be calculated as

$$r_p = \frac{2A_p\left(-D_e \frac{\partial^2 \tilde{C}}{\partial z^2}\bigg|_{z=0}\right)}{A_p(2L_p)} \qquad (22)$$

where A_p is the area of the surface of the particle normal to the z axis. For a bed of depth d_b, void fraction ε_b and having unit width and length, the bed flux (equal to the volumetric uptake rate for a bed of unit width and length) is the product of volume of bed occupied by particles, $(1 - \varepsilon_b)d_b$, and the uptake rate per unit particle volume in equation 22

$$N_b = \frac{(1-\varepsilon_b)d_b}{L_p} D_e \frac{\partial \tilde{C}}{\partial z}\bigg|_{z=0} \qquad (23)$$

The adsorption model requires solution of equation 21 at all axial positions simultaneously with the solution of equation 10. The two solutions are coupled through the boundary condition at z = 0 in equation 21 and the bed

are coupled through the boundary condition at z = 0 in equation 21 and the bed flux given by equation 23. Here there are 5 free parameters--$\rho_p K_d$, L_p, D_e, d_b and ε_b. Fortunately, most of these may be obtained directly for a particular streambed.

Finite Element Solution Technique

The one-dimensional convective-dispersion solute transport model of equation 10 is coupled via the bed flux term to storage models such as the exchange model of equation 12, the diffusion model of equation 14, the underflow model of equation 16, or the adsorption model of equation 21. Because of this coupling, a numerical solution of all model equations is required. Fortunately all the storage models are special cases of the convective-dispersion equation and a method suitable to solve that equation will, with minor modifications, solve all model equations.

Numerical solutions of the convective-dispersion equation are notorious for producing inaccurate representations for sharp concentration fronts, where oscillations and numerical dispersion are commonly observed. This phenomenon is due primarily to the truncation of the high frequency modes by the finite spatial discretization. The finite element method was chosen for this work, where a pulse with sharp leading and trailing edges is to be modeled, as it has been found to be somewhat more accurate than the finite difference method and reduces both numerical dispersion and oscillations (Pinder and Gray, 1976). A Crank-Nicholson or time-centered, time-integration approach was employed, again to reduce numerical dispersion.

The finite element approach requires dividing the spatial domain into an arbitrary but finite number of subdomains referred to as elements. Equation 10 is one-dimensional and hence the spatial domain is a line which may be broken down into n elements, and n + 1 node points. We may then employ an

interpolation scheme to calculate the value of a function at any point on the domain in terms of the values of that function at the node points. Thus, a function (x,t) may be represented as

$$\phi(x,t) = \underline{B}^T(x)\ \underline{\phi}(t) \tag{24}$$

where $\underline{\phi}$ is a column vector containing the n + 1 nodal values of $\phi(x,t)$ and $\underline{B}(x)$ is a column vector of interpolation functions. Note that the nodal values depend only on time and the spatial dependence is contained entirely in the interpolation or basis functions. All functions with spatial variation such as A, C, v, D, d, and N_b can be represented by equation 24.

One is free to employ any reasonable basis functions, $\underline{B}$. The basis functions employed here are the linear basis functions or Chapeau functions which compute an estimate of the function at a point on an element by linear interpolation of the nodal values at the ends of that element. Note that for a given value of x only two basis functions will be non-zero. Thus, if we want an estimate of the value of $\phi(x,t)$ at a point on element i, only $B_i(x)$ and $B_{i+1}(x)$ will be non-zero. These basis functions may be written

$$B_i(x) = \frac{x_{i+1} - x}{x_{i+1} - x_i}$$

$$B_{i+1}(x) = \frac{x - x_i}{x_{i+1} - x_i} \tag{25}$$

where x_i and x_{i+1} are the locations of the nodes terminating element i.

We now employ Galerkin's method, replacing all spatial variables on the lefthand side of equation 10 with the approximation as given in equation 24.

Then the product of the basis functions with the approximation of the lefthand side of equation 10 is integrated over the entire spatial domain from 0 to L. The result is equated to the null vector, $\underline{0}$:

$$\int_0^L \underline{B} \left\{ \underline{B}^T \underline{A} \underline{B}^T \frac{d\underline{C}}{dt} + \underline{B}^T \underline{Q} \frac{d\underline{B}^T}{dx} \underline{C} - \frac{\partial}{\partial x} \left[\underline{B}^T \underline{A} \underline{B}^T \underline{D} \frac{d\underline{B}^T}{dx} \underline{C} \right] + \underline{B}^T \underline{A} \underline{B}^T \underline{S}_b \right\} dx = \underline{0} \qquad (26)$$

where $\underline{Q}$ is a vector containing the nodal values of Av, and $\underline{S}_b$ is a vector containing the nodal values of N_b/d. This equation may be simplified by integrating the dispersion term by parts,

$$\int_0^L \underline{B} \frac{\partial}{\partial x} \left[\underline{B}^T \underline{A} \underline{B}^T \underline{D} \frac{d\underline{B}^T}{dx} \underline{C} \right] dx = \underline{B} \underline{B}^T \underline{A} \underline{B}^T \underline{D} \frac{d\underline{B}^T}{dx} \underline{C} \Bigg|_0^L - \int_0^L \frac{d\underline{B}}{dx} \left[\underline{B}^T \underline{A} \underline{B}^T \underline{D} \frac{d\underline{B}^T}{dx} \underline{C} \right] dx \qquad (27)$$

The first term on the right-hand side of equation 27 represents the difference between the dispersive flux of the species at the upstream boundary and that at the downstream boundary. If we denote these as M_{in} and M_{out} respectively and move them to the right-hand side we obtain

$$\int_0^L \underline{B} \left\{ \underline{B}^T \underline{A} \underline{B}^T \frac{d\underline{C}}{dt} + \underline{B}^T \underline{Q} \frac{d\underline{B}^T}{dx} \underline{C} + \underline{B}^T \underline{A} \underline{B}^T \underline{S}_b \right\} dx + \int_0^L \frac{d\underline{B}}{dx} \underline{B}^T \underline{A} \underline{B}^T \underline{D} \frac{d\underline{B}^T}{dx} \underline{C} \, dx = M_{in} \underline{e}_1 - M_{out} \underline{e}_{n+1} \qquad (28)$$

where $\underline{e}_i$ are the unit basis vectors having all elements equal to zero except the i th with is unity.

Equation 28 may be reorganized by grouping the integrals which multiply $\frac{d\underline{C}}{dt}$ and $\underline{C}$,

$$\left[\int_0^L \underline{B}\,\underline{B}^T\,\underline{A}\,\underline{B}^T\,dx\right]\frac{d\underline{C}}{dt} + \left[\int_0^L \underline{B}\,\underline{B}^T\,\underline{Q}\,\frac{d\underline{B}^T}{dx}\,dx + \int_0^L \frac{d\underline{B}}{dx}\,\underline{B}^T\,\underline{A}\,\underline{B}^T\,\underline{D}\,\frac{d\underline{B}^T}{dx}\,dx\right]\underline{C}$$

$$= -\left[\int_0^L \underline{B}\,\underline{B}^T\,\underline{A}\,\underline{B}^T\,dx\right]\underline{S}_b + M_{in}\underline{e}_1 - M_{out}\underline{e}_{n+1} \qquad (29)$$

All the integrations indicated in equations 29 may be evaluated analytically. Note that the integrals enclosed in brackets will produce matricies and that the integral on the righthand side will produce a vector. The result is the following system of differential equations

$$\underline{\underline{R}}\,\frac{d\underline{C}}{dt} + \underline{\underline{S}}\,\underline{C} = \underline{T} \qquad (30)$$

$\underline{\underline{R}}$ and $\underline{\underline{S}}$ are tridiagonal matricies and $\underline{T}$ is a vector. The evaluation of elements in $\underline{\underline{R}}$, $\underline{\underline{S}}$ and $\underline{T}$ and the modifications necessary to properly impose the boundary conditions are given in the Appendix.

Equation 30 may now be integrated in time using finite difference techniques. The time derivative is approximated using a forward difference,

$$\frac{d\underline{C}}{dt} = \frac{\underline{C}^{j+1} - \underline{C}^j}{\Delta t} \qquad (31)$$

Employing the Crank-Nicholson technique, equation 29 will be evaluated as the centered average of the values at time $t_0 + j\Delta t$ and $t_0 + (j+1)\Delta t$, where

$$\underline{C} = \frac{(\underline{C}^{j+1} + \underline{C}^{j})}{2} \tag{32}$$

Combining equations 30-32 we obtain a system of linear equations for $\underline{C}^{j+1}$,

$$(\underline{\underline{R}} + \frac{\Delta t}{2}\underline{\underline{S}})\underline{C}^{j+1} = (\underline{\underline{R}} - \frac{\Delta t}{2}\underline{\underline{S}})\underline{C}^{j} + \Delta t\,\underline{T}^{j} \tag{33}$$

This system of equations may be efficiently solved using the Thomas algorithm.

All other differential models used here (equations 12, 14, 16 and 21) are special cases of equation 10. This permits a single solution routine to be employed in solving model equations. First, the main stream model and the storage model were solved separately using the value of bed flux, N_b, calculated at the previous time step. The calculated main stream concentrations at each node were compared with the values at the previous time step. If the differences were within a specified tolerance, the results were stored and calculations initiated for the next time step. If any of the mainstream nodal concentration differences were not within the tolerance, new values of the bed flux were calculated for all nodes based on the results of the calculation just completed. The model equations were again solved using the new bed flux values. This process was iterated until the difference between nodal concentrations for successive calculations was within the tolerance for all main stream nodes.

MODEL RESULTS AND DISCUSSION

A. Chloride Transport Modeling

The transport models for chloride tested here represent three different approaches to the bed flux for chloride in the main channel. The exchange model represents both the channel and the bed storage zone as well mixed in the vertical direction and employs a mass transfer coefficient formulation to describe the movement across the bed-stream interface. The diffusion model represents the bed as a stagnant compartment of finite depth into or out of which vertical movement occurs by diffusion alone. The underflow model is actually a hybrid with a source term which includes a contribution from exchange and, at certain nodes, contributions due to loss (or gain) of chloride by advection into (or out of) a separate channel presumed to exist in the bed, i.e. an underflow channel.

The exchange model was suggested by mathematical considerations and the diffusion and underflow models by physical considerations but there was no *a priori* means of knowing which model best represented the actual behavior at Uvas Creek. For that matter, there was no way of knowing whether multiple bed flux mechanisms, some perhaps not even envisaged, contributed to the experimental responses observed at Uvas Creek. Therefore, bed flux models were considered one at a time and the transport model calibrated by optimizing only those adjustable parameters associated with a single bed flux model. The underflow model represents an exception to this because two mechanisms, exchange and underflow, were included. This was necessary because the experimental responses clearly could not be attributed to underflow alone while the abnormal results for both the exchange and diffusion models in the

reach from station 4 to station 5 suggested that additional bed flux mechanisms might exist in that reach. Therefore, exchange was included but only the parameters of the underflow process were varied during calibration.

Before model calibration could begin, it was necessary to determine the dispersion coefficient for each reach. Smith (1970) presented graphical solutions for the convective-dispersion equation without mass generation terms for the case of a step increase in concentration at the inlet. The fraction of the final step increase, C/C_f, observed at distance L from the inlet is a function of the dimensionless time, t/τ, where τ is the mean travel time and a single dimensionless parameter, the Peclet number, N_{Pe},

$$N_{Pe} = \frac{vL}{D} \tag{34}$$

The Peclet number for the stream section from the injection point to the station of interest may be found by plotting the concentration (C) during the arrival of the injected pulse divided by the "plateau" concentration immediately after arrival (C_f). This "plateau" is actually a slowly rising portion of the curve which is due to a slow decrease in discharge during constant injection. This has been done for stations 2-5 in Figure 2. From this figure one concludes that the value of N_{Pe} is nearly constant at a value of about 50. Interestingly this leads to the conclusion that D is not a constant but increases linearly with distance from the injection point, as has been noted by others (Nordin and Sabol, 1974; Day, 1975).

Convective-dispersion models in streams are usually sensitive to dispersion coefficients only when very sharp concentration gradients are passing through the system, hence the determination of a dispersion coefficient may be quite rough. The dispersion coefficient used here was calculated as

$$D = 0.18 + 0.72 \cdot \frac{x}{640} \ \frac{m^2}{sec} \tag{35}$$

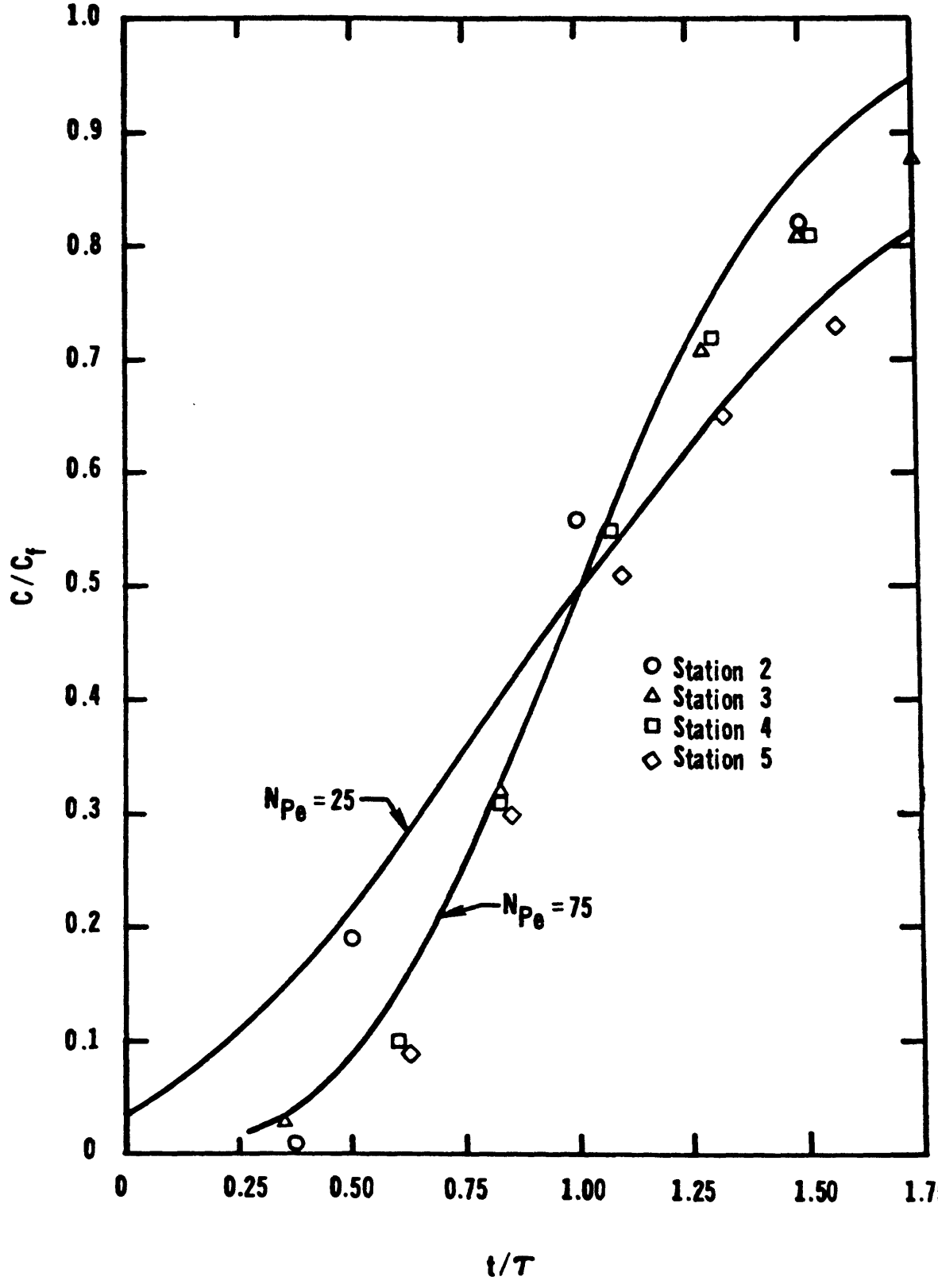

Figure 2. Plot of the concentration ratio, c/c_f, versus t/τ obtained by solving the convective dispersion equation for $N_{pe} = 25$ and $N_{pe} = 75$ (solid lines) compared with actual data for the arrival of the concentration front at stations 2-5.

where x is the distance from the upstream end of the reach in meters. This gives good agreement at station 5 with the value of D obtained by interpolating for N_{Pe} using Figure 2. It gives somewhat higher values of D near the upstream end of the reach but has no observable effect on calculated values except on the rising and falling concentration fronts which passed through the reach. These fronts were not examined during model calibration.

It was hoped that the model calibration would yield information on what processes were actually affecting chloride transport in Uvas Creek. The more nearly the calibrated model predicted observed responses in the creek, the more likely it would be that the model was accounting for the dominant bed flux in the stream. The early numerical results with the exchange model made it clear that excellent agreement could be obtained between model concentrations and experimental concentrations.

Owing to the computational cost associated with model solutions, it was impractical to calibrate models using quantitative goodness of fit criteria and adjusting parameters using multidimensional optimum seeking methods. Therefore, all parameter identifications reported below are based on visual perception of goodness of fit and a rather small number of parameter adjustments.

All parameters in the various storage models were assumed to be constant over a given reach. As parameter choices for an upstream reach affect model predictions in all downstream reaches, it was necessary to find optimal parameters for the most upstream reach first and then search downstream reach by reach. Fortunately much of the rough fitting of parameters in downstream reaches could proceed concurrently with fine-tuning of parameters in an upstream reach.

During the field experiment, cross-sectional areas were measured. Use

of these areas in the simulations yields inconsistent arrival times. Therefore, the cross-sectional area was assumed reachwise constant and reach values were adjusted to produce correct arrival times for the chloride front at each station. Deviations from the measured areas were of the order of 10 percent. As a point of fact it is much easier to determine the average areas by the arrival of the concentration pulse than attempting to measure irregular cross-sectional areas.

i) Exchange model calibration

The exchange model contains only two adjustable parameters, the cross-sectional area of the exchange bed, A_{ex}, and the mass transfer coefficient, k_g. All other parameters were either measured directly or inferred from other experimental observations. A_{ex} and k_g were assumed to be reachwise constant.

An appreciation of the physical implications of the model parameters aids the search for parameter values which will cause the model to best fit the experimental data. The cross-sectional area, A_{ex}, determines storage volume for the reach (A_{ex} times reach length), hence the ultimate storage capability of a reach. The maximum chloride concentration in bed storage cannot exceed that in the stream. Thus, the maximum storage is the product of reach length, the cross-sectional area for exchange (A_{ex}), and the maximum concentration in the stream. Actual storage in the reach at any time depends on how closely the storage concentration follows the stream concentration. The rate of approach of storage concentration to stream concentration is determined by k_g. For a given value of A_{ex}, increasing k_g causes the bed concentration to approach the stream concentration faster and to follow it more closely.

During the period immediately following the passage of the leading edge

of the concentration front, the concentration in the exchange compartment will be low and the flux of chloride into storage will depend almost entirely on k_g. That is, if the predicted concentrations in the main channel are too high (low), only an increase (decrease) of k_g will lower (raise) them. The amount of chloride stored in each reach as the trailing concentration edge passed out of the reach was calculated from mass balances based on the experimental data. If the model predicted more (less) storage and if the storage concentration approached that of the stream, then only a reduction (increase) of A_{ex} could result in agreement. Using reasoning such as this, it was possible to obtain calibrated values of A_{ex} and k_g starting in the first reach and marching progressively downstream.

The initial model calculations employed 102 elements of equal lengths (6.4 m). To reduce the solution cost, this was reduced to a model employing 49 elements, the upstream elements being somewhat shorter than those of the earlier model (6 m) and the downstream elements being considerably longer (25 m). The ability to choose the location of the nodes arbitrarily is in fact one of the powerful aspects of the finite element method. Table 1 gives the node positions and the locations and amounts of apparent ground-water accretion for the 49-element model.

Table 2 gives the diurnal stream discharge at the upstream end of the reach (node 1). Discharge at a particular time was obtained by linear interpolation using values at times before and after the desired time. Table 3 contains the values of cross-sectional area for each reach. Chloride concentration at the upstream injection point was calculated as 0.348 (mg/L) (m^3/sec) divided by discharge at the injection site based on the constant injection rate. Strontium concentration was calculated as 0.0391 (mg/L) (m^3/sec) divided by discharge at the injection site. The downstream boundary

TABLE 1.--Location of finite element network nodes

Node	Distance Downstream From node 1(m)		Ground-water Inflow as Fraction of Upstream Discharge	Node	Distance Downstream From node 1(m)		Ground-water Inflow as Fraction of Upstream Discharge
1	0	(Station 0)	0	27	234	(Station 3)	0
2	6		0	28	249		0
3	12		0	29	264		0.0060
4	19		0	30	279		0.0060
5	26		0	31	294		0.0060
6	33		0	32	309		0
7	40	(Station 1)	0	33	324		0
8	47		0	34	339		0
9	54		0	35	354		0
10	61		0	36	369		0
11	69		0	37	384		0
12	77		0	38	400		0
13	85		0	39	416		0
14	94		0	40	432		0
15	104	(Station 2)	0	41	448	(Station 4)	0
16	114		0	42	465		0
17	124		0	43	483		0
18	135		0	44	502		0.0107
19	146		0	45	522		0.0107
20	157		0.0213	46	544		0.0107
21	168		0.0213	47	567		0
22	179		0.0213	48	591		0
23	190		0	49	615		0
24	201		0	50	640	(Station 5)	0
25	212		0				
26	223		0				

TABLE 2.--Discharge data at Station 1

Time From Start of Injection (hrs)	Discharge (m^3/sec)
-0.0	0.0256
0.5	0.0257
1.0	0.0255
1.5	0.0251
2.2	0.0249
2.5	0.0241
3.3	0.0234
4.0	0.0226
4.7	0.0220
5.3	0.0211
6.0	0.0205
6.7	0.0199
7.3	0.0195
8.0	0.0187
9.0	0.0187
10.0	0.0195
13.0	0.0205
14.8	0.0222
16.7	0.0225
17.7	0.0236
18.7	0.0236
19.7	0.0236
20.7	0.0239
21.7	0.0241
22.7	0.0244
24.7	0.0256

TABLE 3.--Cross-sectional areas for reaches

Reach	Area (m^2)
Injection Site to Station 1	0.304
Station 1 to Station 2	0.415
Station 2 to Station 3	0.336
Station 3 to Station 4	0.368
Station 4 to Station 5	0.404

condition required no dispersive flux. These values were employed for all solutions reported here.

Figures 3a-d show the predictions of the calibrated chloride exchange model at stations 2, 3, 4 and 5 for 30 hours following the start of injection. The values of the adjustable parameters, A_{ex} and k_g are reported in Figure 4a-b. Note that a peak in chloride concentration was observed at all stations. This was caused by the diurnal variation in streamflow coupled with a constant injection rate. Also note that all concentrations reported here are "net", the difference between total concentration and natural background concentration.

The agreement between model predictions and experimental data is in general extremely good. Minor discrepancies at station 2 may be due to experimental errors. The peak concentration observed at station 2 was 18.78 mg/L. This discrepancy is within the experimental uncertainty for the chloride analysis. At station 3 there are again only minor discrepancies between model and experiment. The excellent agreement at stations 2 and 3 for the chloride model argues that the model does very well in describing the convective and dispersive processes. Only about 13 percent of the total storage occurred in the first three reaches (see Figure 5). Any model may permit only small amounts of exchange in these reaches and the agreement between model and experiment is not a sensitive test of the bed storage model. Therefore, in comparing the three different bed storage models studied here, only the agreement between model and experiment at stations 4 and 5 will be considered. Interestingly, the length of the reach from the injection point to station 3 was 37 percent of the total reach from the injection point to station 5. This indicates that the upstream portion was much less active in storing chloride than was the downstream reach.

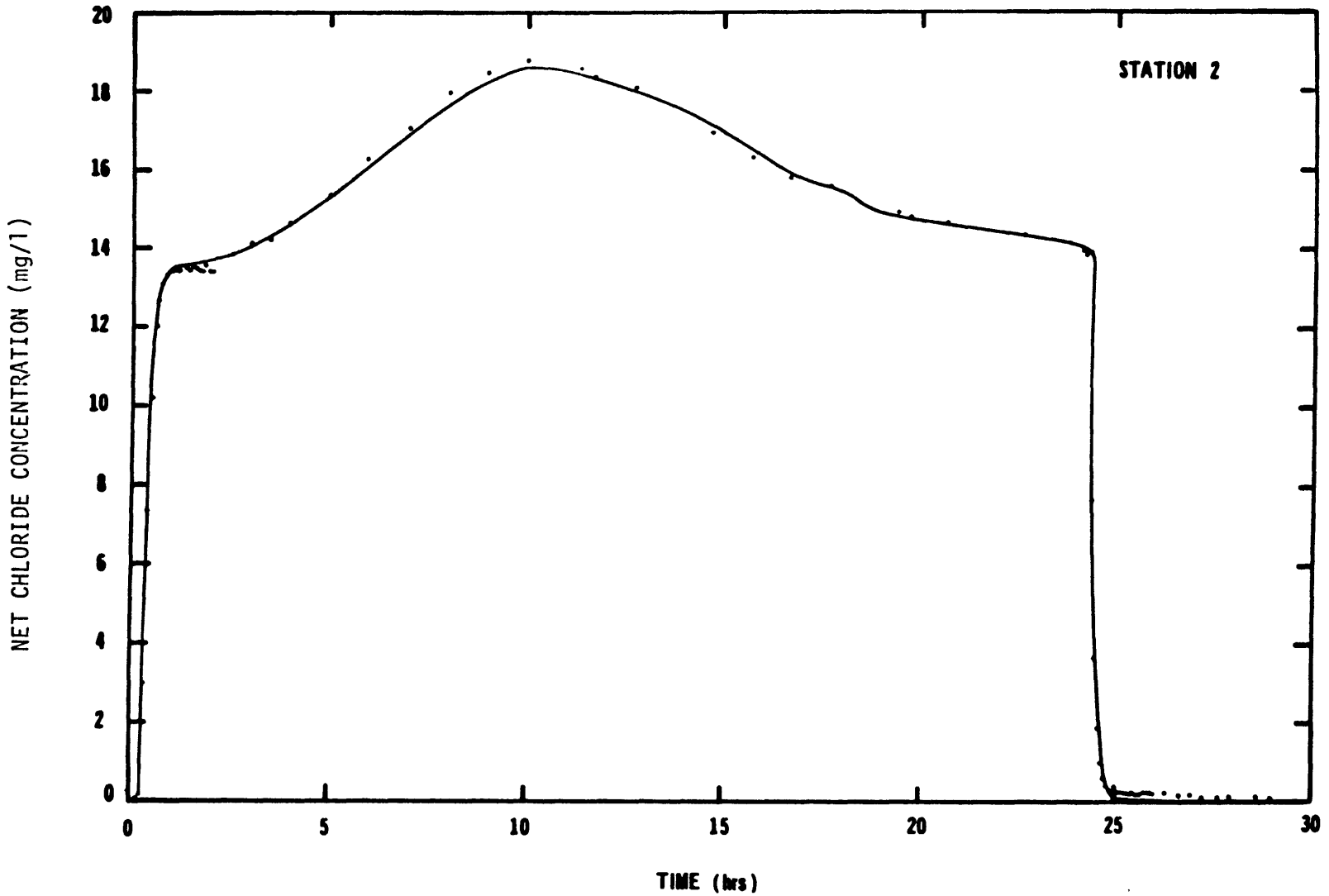

Figure 3a. Comparison of net chloride concentration calculated using the exchange model versus time (solid line) with observed concentrations (dots) at station 2.

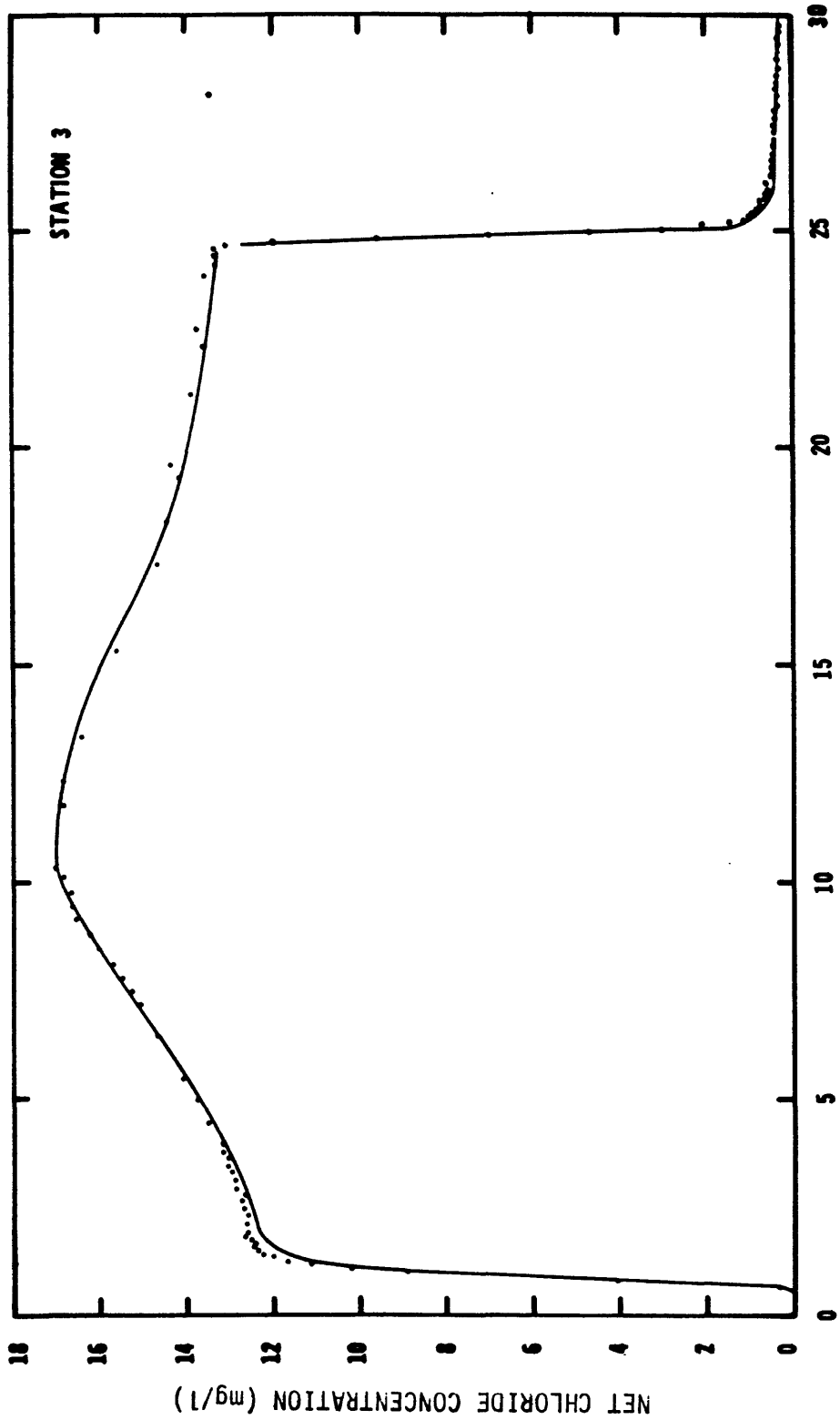

Figure 3b. Comparison of net chloride concentration calculated using the exchange model versus time (solid line) with observed concentrations (dots) at staion 3.

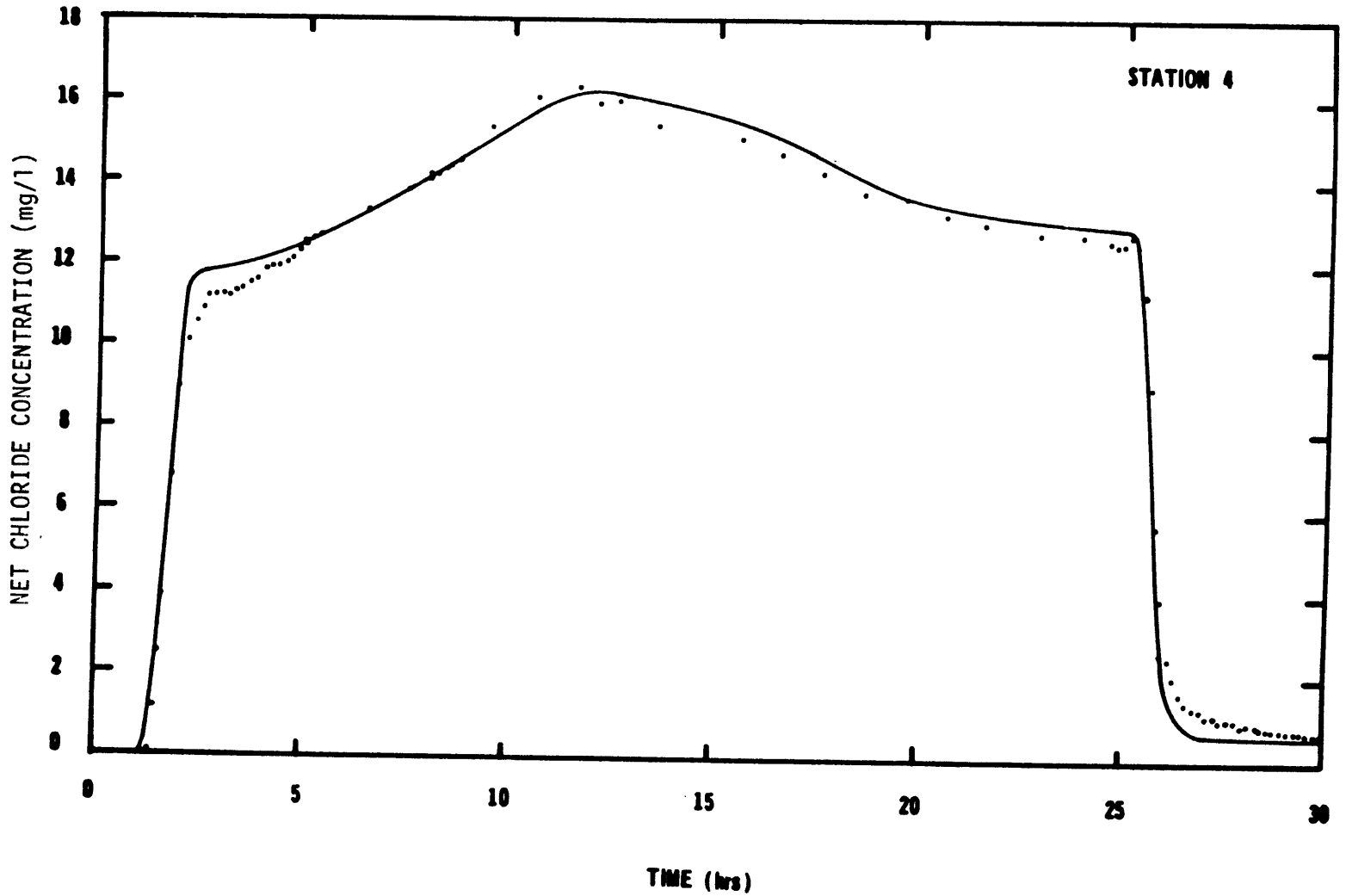

Figure 3c. Comparison of net chloride concentration calculated using the exchange model versus time (solid line) with observed concentrations (dots) at station 4.

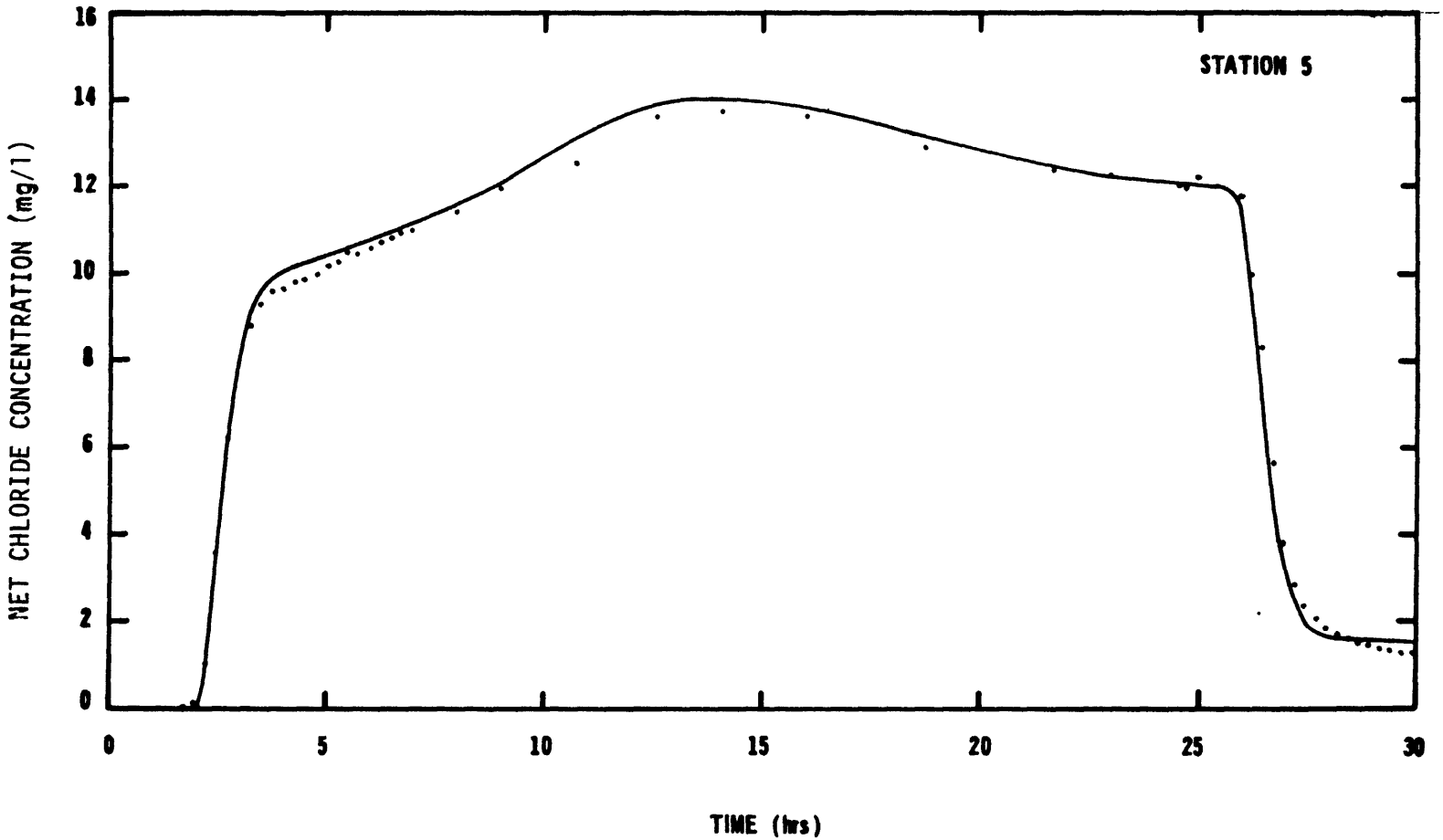

Figure 3d. Comparison of net chloride concentration calculated using the exchange model versus time (solid line) with observed concentrations (dots) at station 5.

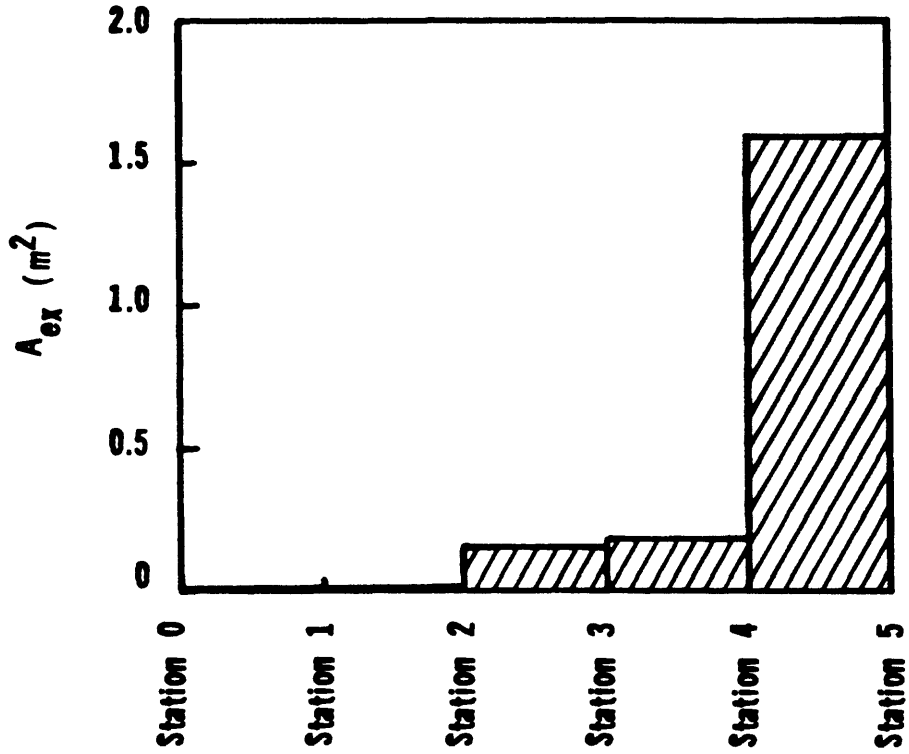

Figure 4a. Fitted values of the reachwise-constant exchange model parameter A_{ex}.

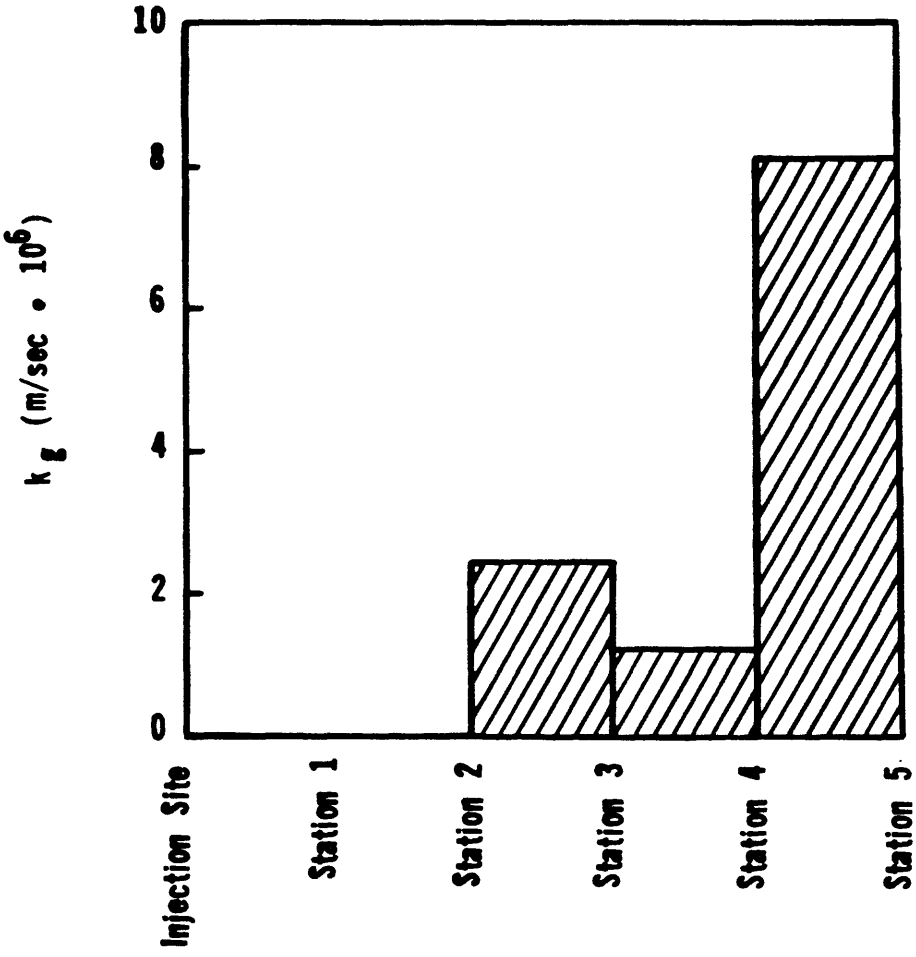

Figure 4b. Fitted values of the reachwise-constant exchange model parameters k_g.

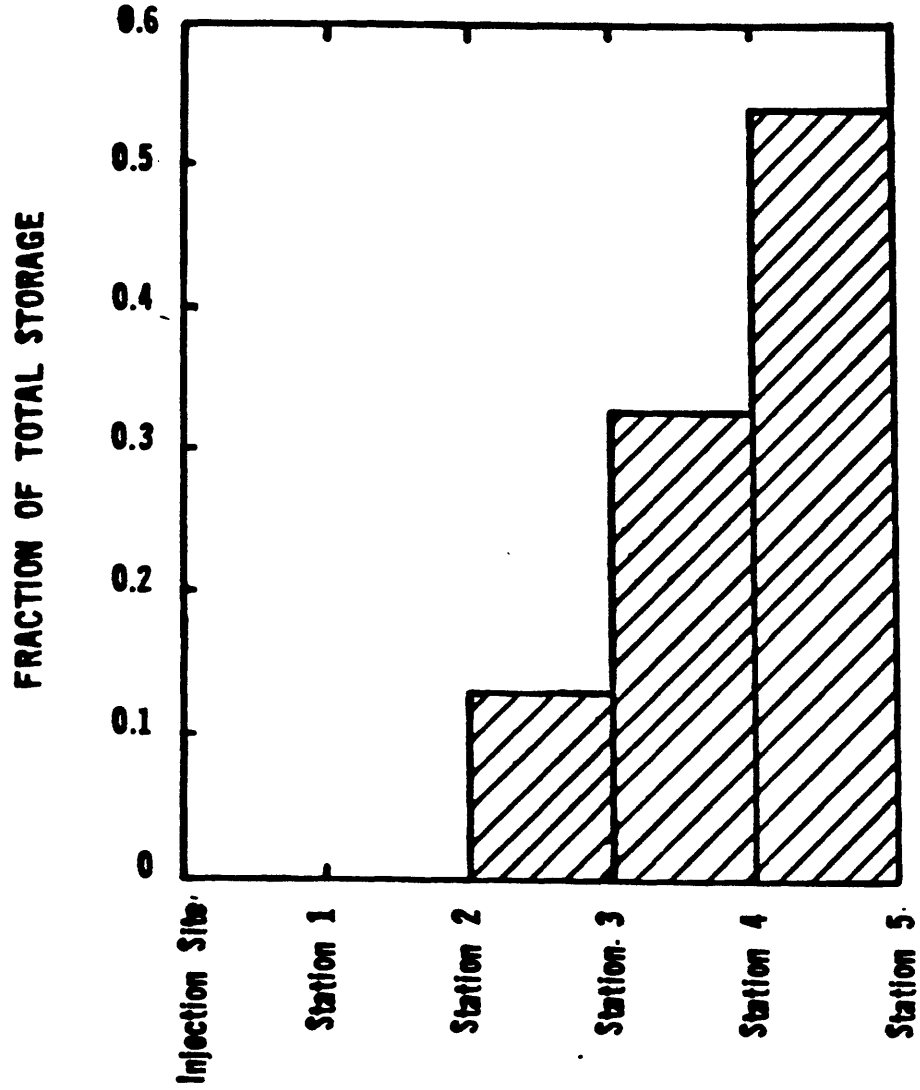

Figure 5. Fraction of total chloride storage on a reach-by-reach basis at the end of the injection period.

Ground-water accretion may have been significant in this part of the stream with channel flow apparently increasing by 6.4 percent in the reach from stations 2 to 3. One possible explanation for the low storage rates in this reach is that the ground water moving through the bed and into the channel prevented the movement of chloride into the bed.

At stations 4 and 5 some minor discrepancies between model and experiment can be seen on careful examination. At both stations, the calculated chloride removal is somewhat less than needed, causing the model to overpredict concentrations. At station 4 the removal is too little for the hours following the peak (hereafter referred to as the "declining phase") and at station 5 the calculated removal rate appears too small over the entire curve. It proved impossible to eliminate these problems with choices of A_{ex} and k_g which predicted peak concentration and the concentrations before the peak (hereafter referred to as the "rising phase"). Nevertheless, the worst discrepancies between model and experiment are only on the order of 0.25 mg/L which is an error of only 2 percent of the observed net chloride concentration.

The reach from stations 4 to 5 is of great interest in studying chloride bed flux terms because 54 percent of all chloride in storage at conclusion of the injection was stored in that reach. Downstream restorage of chloride released from storage in upstream reaches increases the significance of the uptake processes in this reach.

The large variation of model parameters from reach to reach is notable. Such results are not unexpected for short reaches of cobble-bed, pool-and-riffle streams in mountainous terrain. The distribution of pools and riffles was uneven between reaches and the permeability of the bed was almost certainly highly variable, particularly where the stream abutted

outcropping bedrock. We would expect less variability when averaged over longer reaches.

ii) Diffusion model calibration

The bed flux term for the diffusion model is given by equation 13. This model contains only two adjustable parameters, the bed depth, d_b, and the effective diffusivity for the bed, D_b. The model assumes that diffusion into the bed is the only operative transport mechanism, there being no bed convection, either vertical or axial. The model employs an initial condition of no chloride in the bed. The boundary condition at the bed-stream interface fixes the chloride concentration at the bulk stream concentration. And the boundary condition at the bottom of the bed forbids chloride flux out of the bed.

Computationally, the diffusion model is considerably more complex than the exchange model. This is caused by the pseudo-two-dimensional nature of the model. For each node in the stream there must be an array of vertical elements representing the bed at that point. To reduce the computation time, each vertical array consists of only 4 elements. To improve the accuracy, the length of these elements is allowed to increase considerably with depth, the element lengths being 1/15, 2/15, 4/15 and 8/15 of the total bed depth respectively.

Before solving the main stream problem, values of the bed flux at each axial node must be available. Therefore, the solutions for all the vertical arrays were generated before starting the solution of the axial arrays. This requires use of the mainstream concentration at the previous timestep as the boundary condition on the bed array. If iteration is required, subsequent boundary values are taken as the mainstream concentration at the previous

iteration.

After solving for all vertical arrays, the bed flux at each axial node may be calculated and then the new concentrations at the axial nodes determined. In the results reported here, iteration was performed only if the previous concentration at one of the axial nodes differed by more than 0.5 mg/L from the current solution.

As with the exchange model, an appreciation of the physical implications of the adjustable parameters is an aid in searching for optimal parameters. For very low values of the bed diffusivity, D_b, the concentration at the bottom of the bed will not be appreciable and the total bed depth, d_b, has no effect on the solution. For higher values of D_b, the bed depth does not affect the model results until the concentration at the bottom of the bed does become appreciable, after which d_b controls storage volume, hence total reach storage. Thus, D_b may be found independently during the first few hours of the simulation. Having found D_b in this way, d_b may be adjusted to force the correct amount of chloride to be stored in each reach as the trailing edge of the concentration front passed out of that reach. Equivalently, it may be adjusted to give good agreement between model and experiment during the declining phase. The latter technique was used here. The ability to separate the identification of the two model parameters greatly speeds the identification process. The values of the adjustable parameters, d_b and D_b, are given in Figure 6 a-b. The agreement between model and experiment is closely similar to that found for the exchange model in Figures 3a-d; hence separate figures are not shown. A more detailed comparison of the two models will be given below.

Previous experience with the exchange model had shown that little or no uptake occurred in the reach from the injection point to station 2. For the

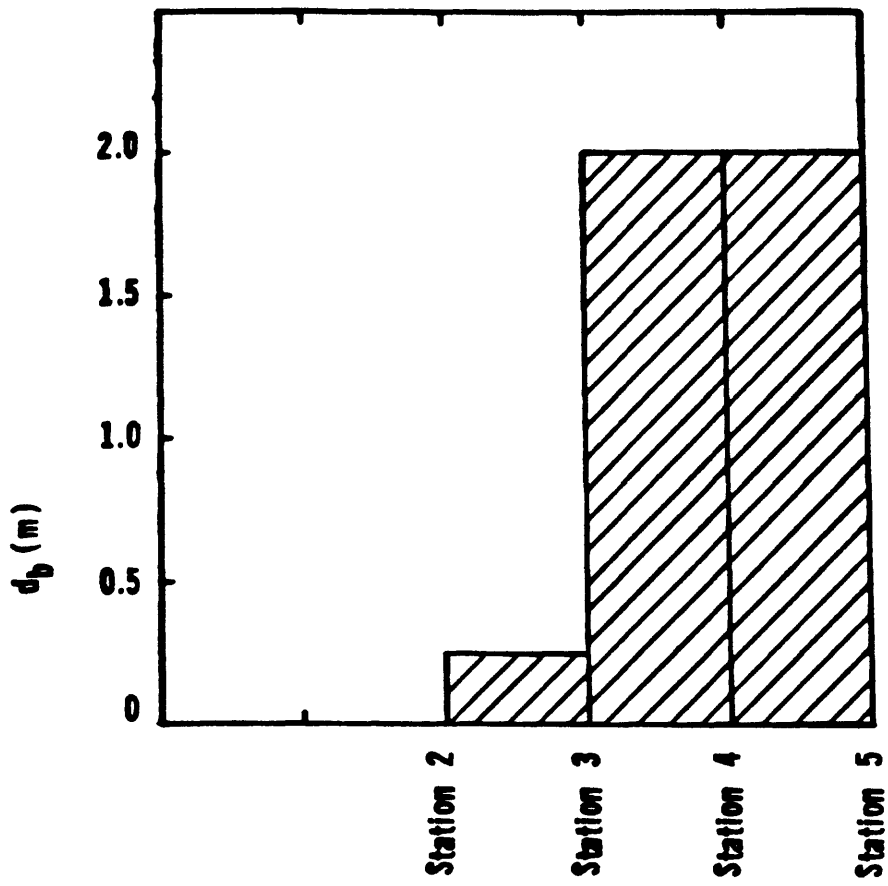

Figure 6a. Fitted values of the reachwise-constant diffusion model parameter d_b.

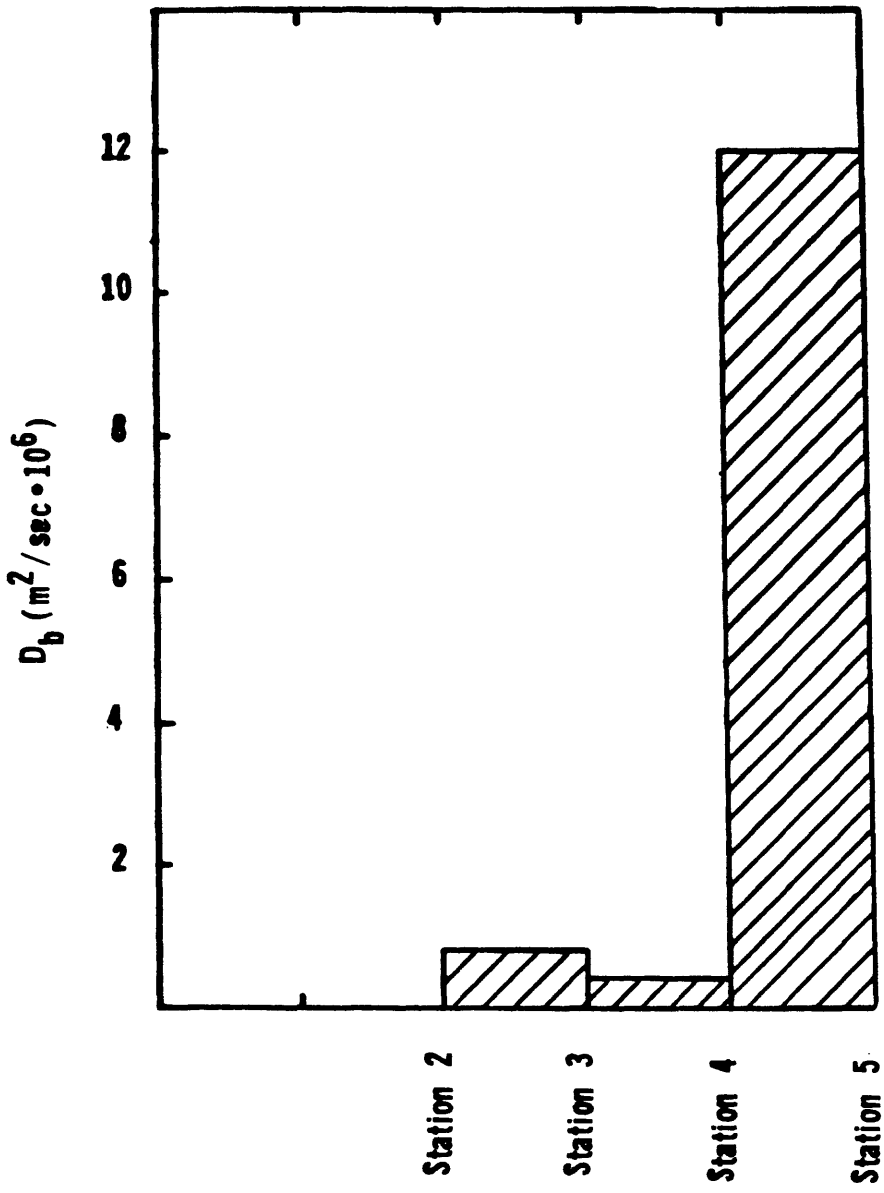

Figure 6b. Fitted values of the reachwise-constant diffusion model parameter D_b.

diffusion model, computational time was saved by solving the bed arrays only from station 2 to station 5, ignoring storage upstream of station 2.

The great disparity between the reach from station 4 to 5 and the remainder of the reach is again obvious. The diffusion coefficient for this reach was found to be more than an order of magnitude greater than that for any other reach. The depth of the bed in this reach is also very great, being eight times the depth found for the reach from station 2 to 3. The depth parameter has little effect on the solution for the reach from station 3 to 4. The best fit for this reach simply required a depth great enough to allow no appreciable concentration buildup to occur at the bottom of the bed.

As with the exchange model, the agreement between model and experiment is good. It is possible to discern minor differences between the fit obtained with the two models. At stations 4 and 5 some small differences attributable to the models appear. The diffusion model exhibits high initial uptake which must decrease rather rapidly as the upper structure of the bed becomes saturated with chloride. With the exchange model, uptake remains fairly constant during the first few hours as the bed is assumed to be well mixed, which requires that the concentration in the entire bed structure build. For this reason, the exchange model slightly overpredicts (too little uptake) the stream concentrations for the first few hours at both stations 4 and 5 whereas the diffusion model underpredicts (too much uptake). At station 5 this comparison tends to favor the exchange model.

For the optimal fit with the exchange model, the declining phase concentrations drop off too slowly. This is due to the relatively low bed concentrations which are required to fit the rising phase. A more nearly correct declining phase slope will result in significant overestimation of peak concentrations. The diffusion model does considerably better here,

allowing a good fit at the peak and to the declining phase at the expense of the rising phase.

iii) Underflow model calibration

The underflow model tested here is basically the exchange model with the addition of a single underflow channel in which the only operative processes are diffusion and convection. As discussed above, the model was tested because 1) there are places in the reach where it appears that appreciable bed flow could occur and 2) such a process will tend to cause a larger increase in uptake rate to occur during the rising phase. Unfortunately there is little basis for choosing some of the many parameters involved in such a model. The adjustable parameters for the underflow channel are the channel length and cross-sectional area, the dispersion coefficient for the channel and the volumetric flowrate. In addition, it is necessary to specify the point in the main channel where flow enters the underflow channel and the point where the underflow returns to the main channel. Thus, there are, in a sense, 6 adjustable parameters in the model.

The residence time for the underflow channel should be such that the underflow begins returning chloride to the main channel near the time of the concentration peak. This will cause the underflow to appear as a sink during the rising phase (i.e., between the initial shoulder on the concentration-vs.-time plot and maximum concentration), but to have little influence during the declining phase (i.e., between maximum concentration and the second shoulder on the concentration plot) as the underflow return will have roughly as much chloride as the main channel. This requires a residence time of about 14 hours.

In order to permit another sink term, the uptake due to exchange must be reduced. Uptake in the reach from stations 4-5 was much larger than that for others, therefore the underflow return was chosen to occur in this reach and the value of k_g for this reach was reduced (arbitrarily) to half the value used for the exchange model. The point of underflow return was sited toward the upstream end of that reach at 465 meters. The source of the underflow was taken to be at 432 meters.

At the end of the injection period, the storage in the underflow channel must be large enough to make up for the chloride which was not stored by the exchange process as a result of the reduction of k_g. With k_g of $4.08 \cdot 10^{-6}$ m/sec in the final reach, the required volume of the underflow channel is on the order of 75 m^3. Rather arbitrarily, the length of the underflow bed was set at 40 m, requiring a cross-sectional area of approximately 1.9 m^2.

Due to the number of adjustable parameters, no attempt was made to find an optimized parameter set. However, some attempts were made to identify realistic values for the bed cross-sectional area, the dispersion coefficient and the volumetric flow rate. The values of all adjustable parameters used for the simulations discussed below are given in Table 4.

iv) Comparison of model results

As noted above, the three models for chloride bed storage all predict the observed chloride concentration as a function of time with impressive accuracy. In fact, the agreement is so good that only with great care can one distinguish between the predictions of any two models at any of the stations during the passage of the 24-hr wide pulse.

Therefore an attempt was made to find more sensitive measures of predictive value of the models. Because model calibration was performed

TABLE 4.--Underflow channel parameters

L_u = 40 m

A_u = 1.85 m^2

Q_u = 1.42 10^{-3} m^3/sec

D_u = 20 10^{-6} m^2/sec

using only those data collected during the passage of the pulse, comparison of the model predictions after passage of the pulse offers one such opportunity. Extensive data were collected on the tail of the concentration die-away curve, particularly at station 5 where chloride was greater than 0.10 mg/L above background for at least 3 days following the cutoff of the injection and where differences greater than the precision level of the chemical analysis for chloride (~0.03 mg/L) were observed for at least 2 weeks following the cutoff. During this period the model is required to predict the release of chloride from bed storage as well as transport and restorage of released chloride.

In modeling the storage and transport after injection cutoff, it was assumed that the diurnal pattern of stream discharge was that observed on the day of the injection. Stage records collected at the Parshall flume support this assumption. The diurnal pattern was observed with little difference in magnitude from day-to-day and the mean daily discharge declined only slightly during the period. In particular, we will concern ourselves here with the first 72 hours following injection cutoff which saw very little change in discharge pattern.

Figure 7 shows the predictions for the exchange model, diffusion model and underflow model at station 5 together with actual data collected there for a period of about 3 days following the cutoff of the injection. In this form, model differences are readily seen. Out to about hour 72 the exchange model appreciably overpredicts chloride concentration and thereafter it slightly underpredicts. This indicates that the exchange model is over-predicting the rate of return of chloride stored in the bed until a rather low level on the tail is reached.

The diffusion model should respond more rapidly to rapid changes in main

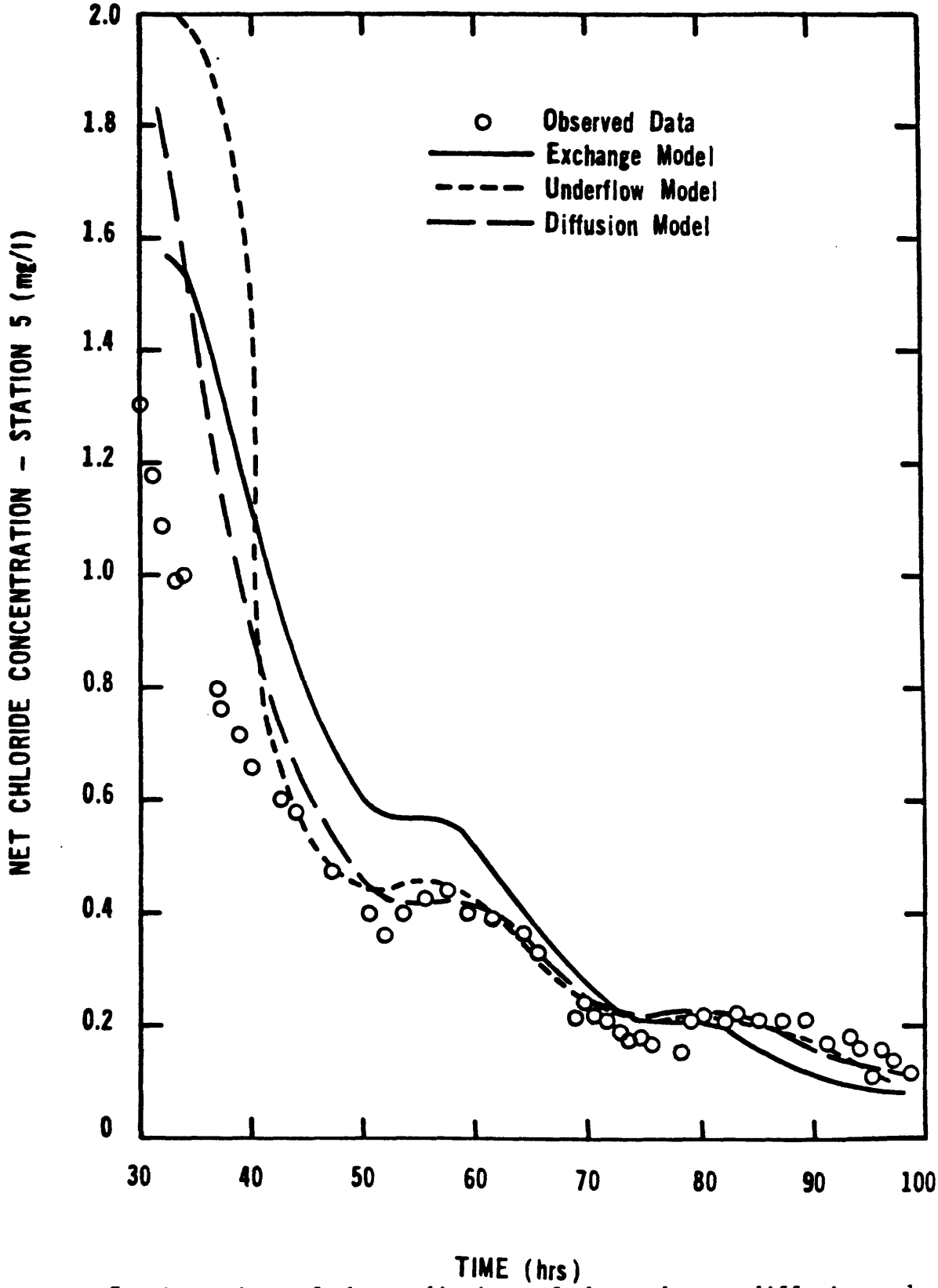

Figure 7. Comparison of the predictions of the exchange, diffusion and underflow model predictions for station 5 with the observed data for the period from hour 30 to hour 100.

stream concentration. We noted earlier that the diffusion model slightly underpredicted stream concentrations during the early phases of the injection, indicating that storage was occurring at a slightly higher rate than actually occurred. Here we see that during the early phases of the tail the diffusion model is overpredicting stream concentration indicating a high rate of release from storage. However, by hour 34 the diffusion model has dropped below the exchange model and from hour 40 the agreement between model and experiment is good.

The underflow model greatly overestimates the early phases of the tail. This is caused by the fact that the underflow channel continues to return water of high concentration for one hydraulic residence time (14 hrs) of the underflow channel following passage of the trailing edge of pulse by the inlet to the underflow channel. At hour 40 the predicted concentration drops dramatically as the last of the high-chloride underflow returns to the mainstream. Thereafter, agreement between model and experiment is exceptionally good.

All three models predict either a brief cessation of decline or a slight rise in stream concentration during the afternoon. This corresponds to the period of low discharge which occurs each afternoon. These may be seen around hours 54 and 78. This artifact of the model may also be seen in the data around hour 78. This is strong evidence for the accuracy with which the convective term is being modeled.

Another sensitive comparison of the models is based on the apparent rate of storage of chloride during passage of the pulse. The "fractional uptake" of chloride, defined as the fraction of the chloride concentration, possessed by a packet of water as it passed station 3 at time t, which had been lost as the same packet passed station 5 at $t + \tau$ where τ is the travel time from

station 3 to station 5. It should be noted that not all the fractional uptake is due to bed storage. Based on possible ground-water inflow we expect a decrease (fractional uptake) of about 0.05.

The observed fractional uptake as well as the fractional uptakes for the three models are presented in Figure 8. The observed fractional uptake increases slightly following the start of injection, reaching a maximum of 0.16 at about hour 10. Thereafter it declines rapidly, dropping to about 0.05 at hour 24. This indicates that storage had nearly ceased for packets moving down the reach near the end of the injection period, and observed fractional uptake could be accounted for nearly entirely by ground-water inflow.

This slight initial rise in fractional uptake is most closely approximated by the exchange and underflow models. This is the result of an increase in the driving force for storage, $C - C_b$, during the early stages of the injection. At this time, the stream concentration, C, was rising faster due to diurnal discharge decline than the storage concentration, C_b, was rising due to movement of chloride into the bed. The inclusion of an underflow channel slightly accentuates this rise in fractional uptake until chloride-rich underflow return occurs about one underflow residence time later.

The diffusion model is unable to reproduce the early rise in the observed fractional uptake. This model predicts that the highest rate of storage occurs as the leading edge of the concentration pulse passes through the reach. It is during this period that the gradient in concentration at the streambed interface, $\left(\frac{\partial c}{\partial z}\right)_{z=0}$ is maximum and therefore the rate of uptake is greatest.

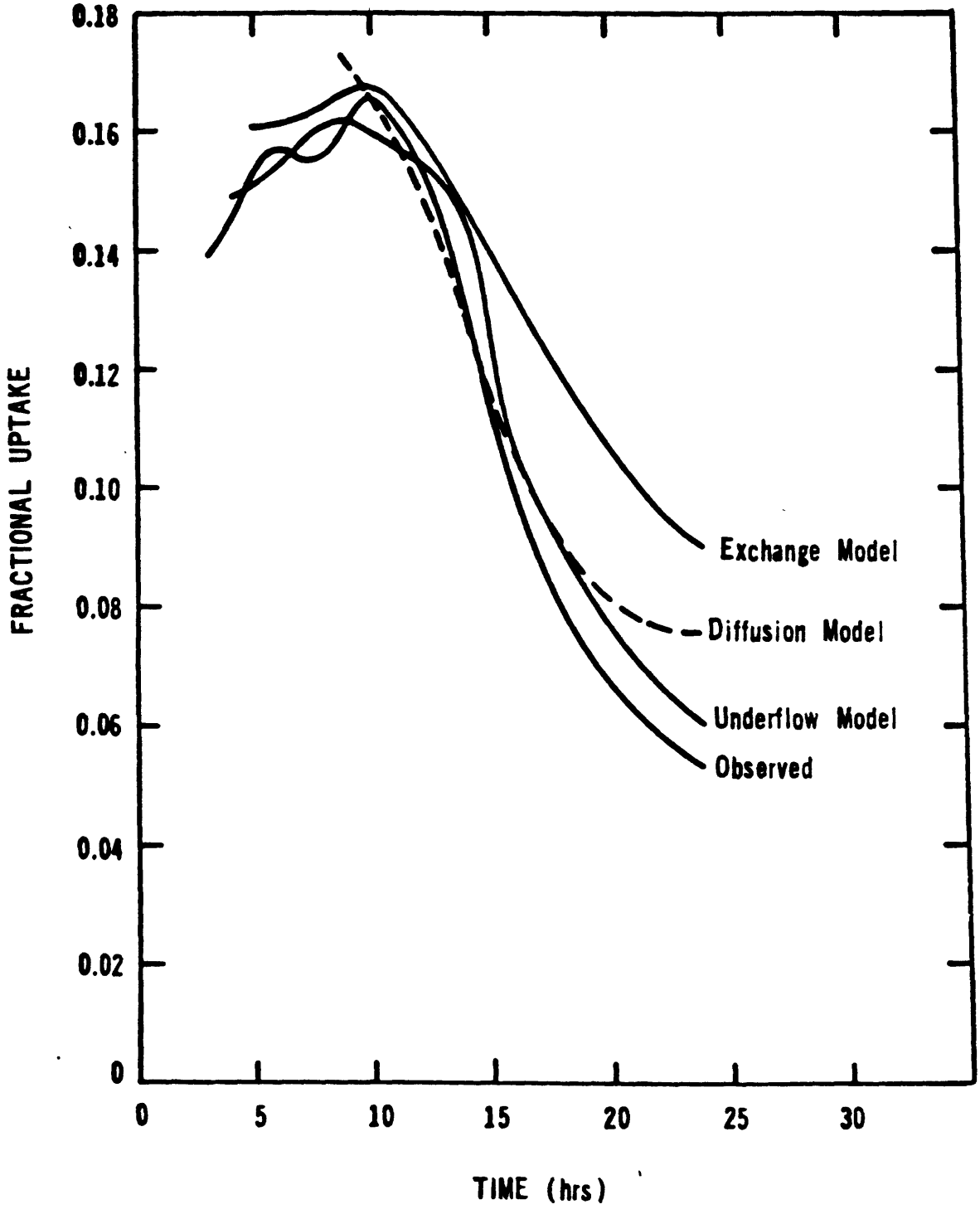

Figure 8. Comparison of predicted fractional uptake (see text) for the exchange, diffusion and underflow models with the observed fractional uptake.

Following the maximum at about hour 10, the observed fractional uptake enters a prolonged decline. Initially the decline in fractional uptake is rapid but the decline slows near the end of the injection. This decline may be attributed to two factors: the storage becomes nearly saturated with chloride near the end and the stream concentration decreases in the early morning hours due to the diurnal discharge increase.

All three models predict a substantial decline in fractional uptake. The diffusion model most closely predicts the shape and magnitude of the decline. The exchange model considerably overpredicts the fractional uptake during this period. The underflow model improves considerably on the exchange model during this phase because the underflow becomes totally saturated during this period, producing a rapid decline in fractional uptake as high concentration underflow return begins.

The examination of the tail of the concentration pulse and the fractional uptake during pulse passage provides the best test of the predictive ability of the models and some physical insight regarding actual storage mechanisms. Clearly, the diffusion and underflow models are superior to the exchange model in both these respects. The inability of the diffusion model to predict the observed increase early in the injection argues that other mechanisms must have been contributing to storage. However, the underflow model with its six adjustable parameters must be considered too difficult to calibrate to be of use in routine solute transport modeling. It is of interest here as considerable evidence points to the existence of such a mechanism and because such a mechanism could account for the retention of a large fraction of the strontium in the reach weeks after the injection terminated. This will be discussed further below.

Practical considerations suggest use of the diffusion or exchange

models. Based on the Uvas Creek experiment, we would conclude that the diffusion model is superior although computationally more difficult. Further testing is required to determine the generality of this observation.

All three storage models described above are able to adequately simulate the significant features of the observed concentration data reasonably well. In particular, they are predicting a significant reduction in peak Cl levels with position downstream due to assumed movement of solute into temporary bed storage. This feature could be reproduced by increasing ground-water inflow although the shape of the peak would not fit the data as well, overestimating concentration during the rising phase and underestimating it during the declining phase. But, without the storage, the tail would be nearly eliminated, in disagreement with the observed data.

B) Strontium Transport Modeling

The divalent strontium cation, Sr, is known to adsorb on most streambed materials composed of clay minerals (Shih and Glogna, 1969; Malcolm and Kennedy, 1970). For concentrations on the order of 2 mg/L as were employed at Uvas Creek, the predominant adsorption mechanism is probably ion exchange. To facilitate modeling this reactive bed process, independent studies of the ion-exchange characteristics of bed materials were undertaken both in the laboratory and the field.

A representative sample of Uvas Creek bed material was wet sieved to obtain particles in the following size ranges: 210-250 μm, 420-500 μm, 841-1000 μm, 1680-2000 μm and 3360-4000 μm. This material was placed in porous polyester bags. Forty-two bags of each particle size were placed on the streambed below station 2 prior to the start of the injection. After the start of the injection these bags were retrieved from the streambed, washed

very briefly with distilled water to remove interstitial solutes and returned to the laboratory. Adsorbed Sr was desorbed using 1 N ammonium acetate and determined by atomic absorption spectrometry.

For all size ranges, the quantity adsorbed was assumed to have reached a plateau value prior to the cutoff of the injection. Dividing the plateau absorbate concentration in grams of Sr per gram of adsorbent by the nearly constant concentration of Sr in the stream at station 1, the strontium distribution coefficient for each size range may be calculated. Values of K_d ranged from $5.2 \cdot 10^{-5}$ m^3/g for the 841-1000 μm material to a low of $2.2 \cdot 10^{-5}$ m^3/g for the 3360-4000 μm material. For the modeling reported here, a value of $K_d = 4.10^{-5}$ m^3/g was employed.

The effective diffusivity, D_e, can be estimated from the transient adsorption data obtained from the bag samples. Assuming the particles to be spherical and pseudo-homogeneous, that Sr in the pore fluid is at all times in equilibrium with Sr adsorbed on the adjacent solid phase and obeys the linear isotherm of equation 17 and that accumulation in the pore fluid is negligible compared to accumulation on the adjacent solid ($\rho_p K_d >> \varepsilon_p$), we may describe the movement of Sr in the pores by

$$\rho_p K_d \frac{\partial \tilde{C}}{\partial t} = D_e \frac{1}{r^2} \frac{\partial}{\partial r} \left(r^2 \frac{\partial \tilde{C}}{\partial r} \right) \qquad (36)$$

$$\tilde{C} = 0 \qquad \text{at } t=0 \quad 0 \leq r \leq R$$

$$\tilde{C} = C_{res} \qquad \text{at } r=R \quad t>0$$

$$\frac{\partial \tilde{C}}{\partial r} = 0 \qquad \text{at } r=0 \quad t>0$$

where C_{res} is the fluid concentration in the well mixed reservoir which obeys

$$\frac{dC_{res}}{dt} = -\frac{3(1-\varepsilon_b)V_{bed}}{V_{res}} \frac{D_e}{R} \frac{\partial \tilde{C}}{\partial r}\bigg|_{r=R} \qquad (37)$$

$$C_{res} = C_o \text{ at } t=t_o$$

where ε_b and V_{bed} are the void fraction and total volume of the sample in the tube. The solution to equations 36 and 37 may be shown (Bird, Stewart and Lightfoot, 1959, p. 357-360) to be

$$C_{res} = C_o \left[\frac{B}{B+1} + 6B \sum_{k=1}^{\infty} \frac{\exp\left(\frac{-b_k^2 D_e t}{\rho_p K_d R^2}\right)}{B^2 b_k^2 + 9(1+B)} \right] \qquad (38)$$

where

$$B = \frac{V_{res}}{(1-\varepsilon_b)V_{bed}\,\rho_p\,K_d}$$

and b_k are roots of $\tan b = \frac{3b}{3+b^2B}$

Using $K_d = 4 \cdot 10^{-5}$ m^3/g and a typical particle density of $\rho_p = 2.5 \cdot 10^6$ g/m^3, the effective diffusivity, D_e, for several sizes of particles, was determined by fitting measured uptake data to equation 38. A typical value of D_e was found to be $D_e = 3 \cdot 10^{-9}$ m^2/sec. These values for ρ_p, K_d and D_e were used for all model results reported here. A value of 0.3 was used for ε_b.

The free parameters in the adsorption model are K_d, D_e, ρ_p, L_p, ε_b, and d_b. We have now estimated all of these parameters except L_p and d_b, leaving these parameters free to fit the adsorption model to the Uvas Creek data.

The particle half thickness, L_p, will determine the time course of the adsorption uptake process. The amount stored at any time is determined by both the particle half thickness and the bed depth as the entire bed to depth d_b is assumed to participate equally. Fortunately, the entire bed was found to approach saturation near the end of the injection for reasonable values of L_p. Thus, d_b was adjusted to obtain the observed storage of Sr for a given reach near the end of the injection and L_p was adjusted to obtain the best possible representation of concentration versus time during the passage of the injection pulse.

Figure 9 contains the fitted values of d_b found for each reach as well as the fitted value for L_p which was taken to be the same for all reaches. Note that variation of bed depths from reach to reach is similar to that found for both the exchange and diffusion chloride (conservative) models except that the values for the reaches from 0 to 1 and 1 to 2 are greater relative to values in downstream reaches for Sr. The upstream two reaches appear to be much more active for ion-exchange than for chloride storage.

A comparison of model predictions with experimental data during the

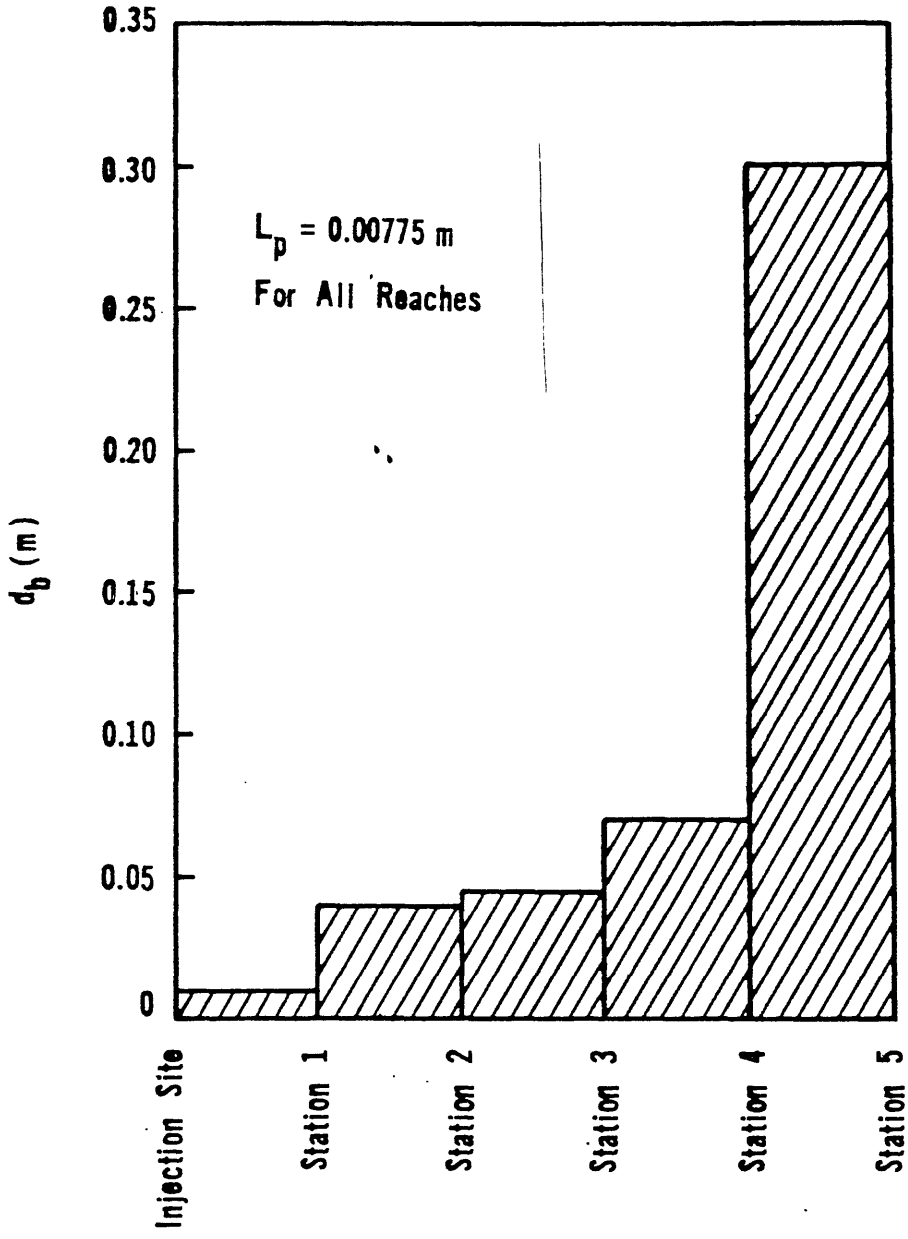

Figure 9. Fitted value of the reachwise-constant adsorption model parameter d_b.

passage of the pulse is shown in Figure 10. Agreement at stations 2 and 3 is excellent. At station 4 it was not possible to find values for L_p and d_b which would cause the model to agree with experiment near the end of the pulse without a serious underestimation near the start of the pulse. The fitted solution underestimates the concentration during the first half of the pulse passage. The same behavior is even more clearly shown in the results for station 5. At station 5 the model prediction is nearly 30 percent low as the pulse arrives although the model and experiment agree to within 5 percent for most of the pulse passage.

The adsorption model is clearly overestimating the rate of removal of Sr during the period immediately following the initial arrival of the concentration pulse. One possible explanation might be that during this period, only a fraction of the bed is really participating in the adsorption process because of the limited rate at which Sr can diffuse into the bed structure. This points out the weakness of the model assumption which takes the bed to be uniform over the entire bed depth, d_b.

Figure 11 compares the observed tail of the Sr pulse with that predicted by the model out to 72 hours following cutoff. The model considerably overpredicts concentrations in the tail. This difficulty was expected. The adsorption model employed here is fully reversible. Hence, all the injected strontium must be either convected out of the reach during the passage of the pulse or adsorbed onto the sediments and gradually released after the pulse passage in the form of a long tail. A careful comparison of the experimental data on strontium injected at station 0 and leaving at station 5 shows that about 32 percent of the material injected remained in the reach 3 weeks after the injection. It appears that this material was either irreversibly bound to the bed or was trapped in underflow channels within the bed where, due to

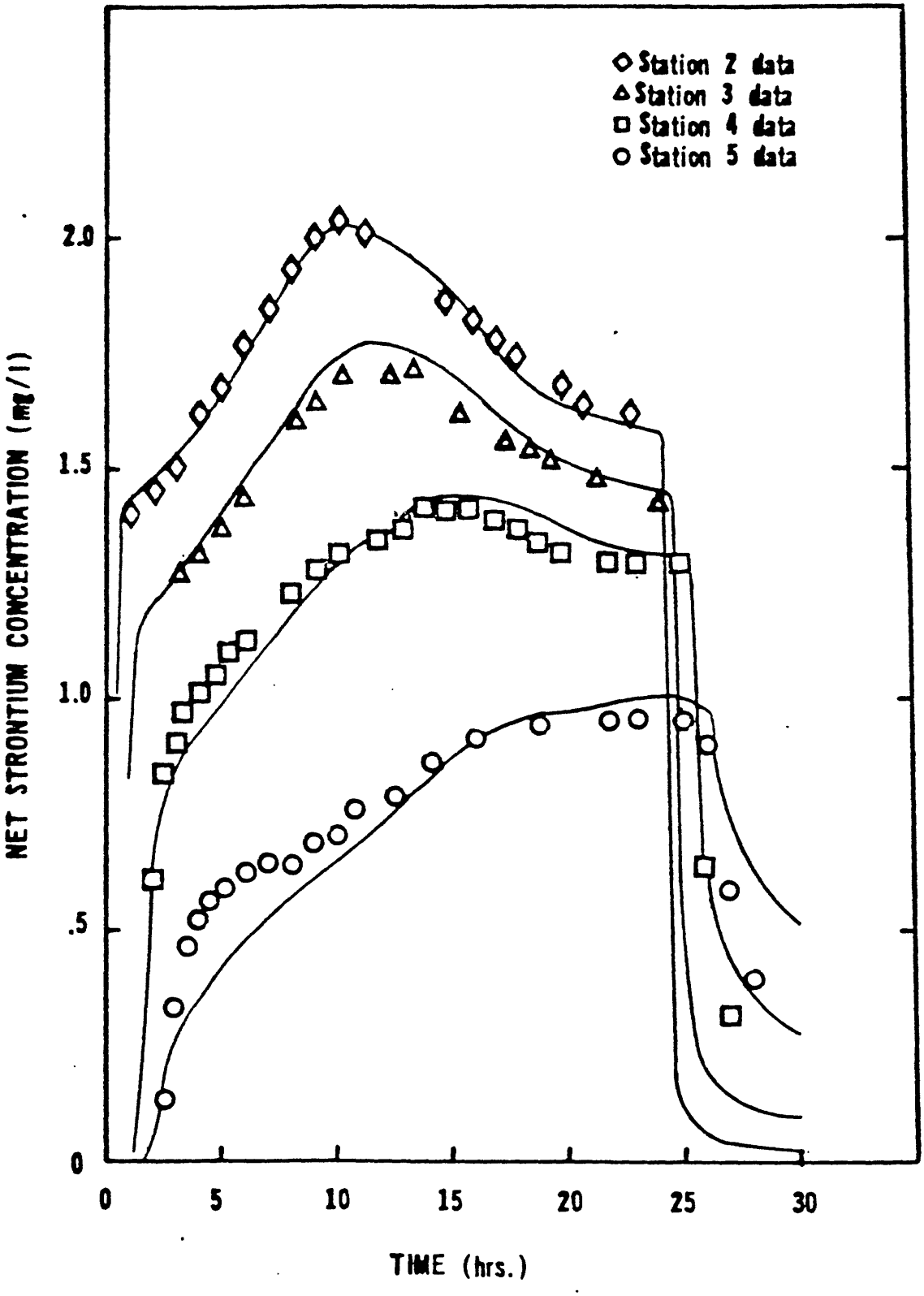

Figure 10. Comparison of net strontium concentration calculated using the adsorption model with observed concentrations for stations 2, 3, 4, and 5.

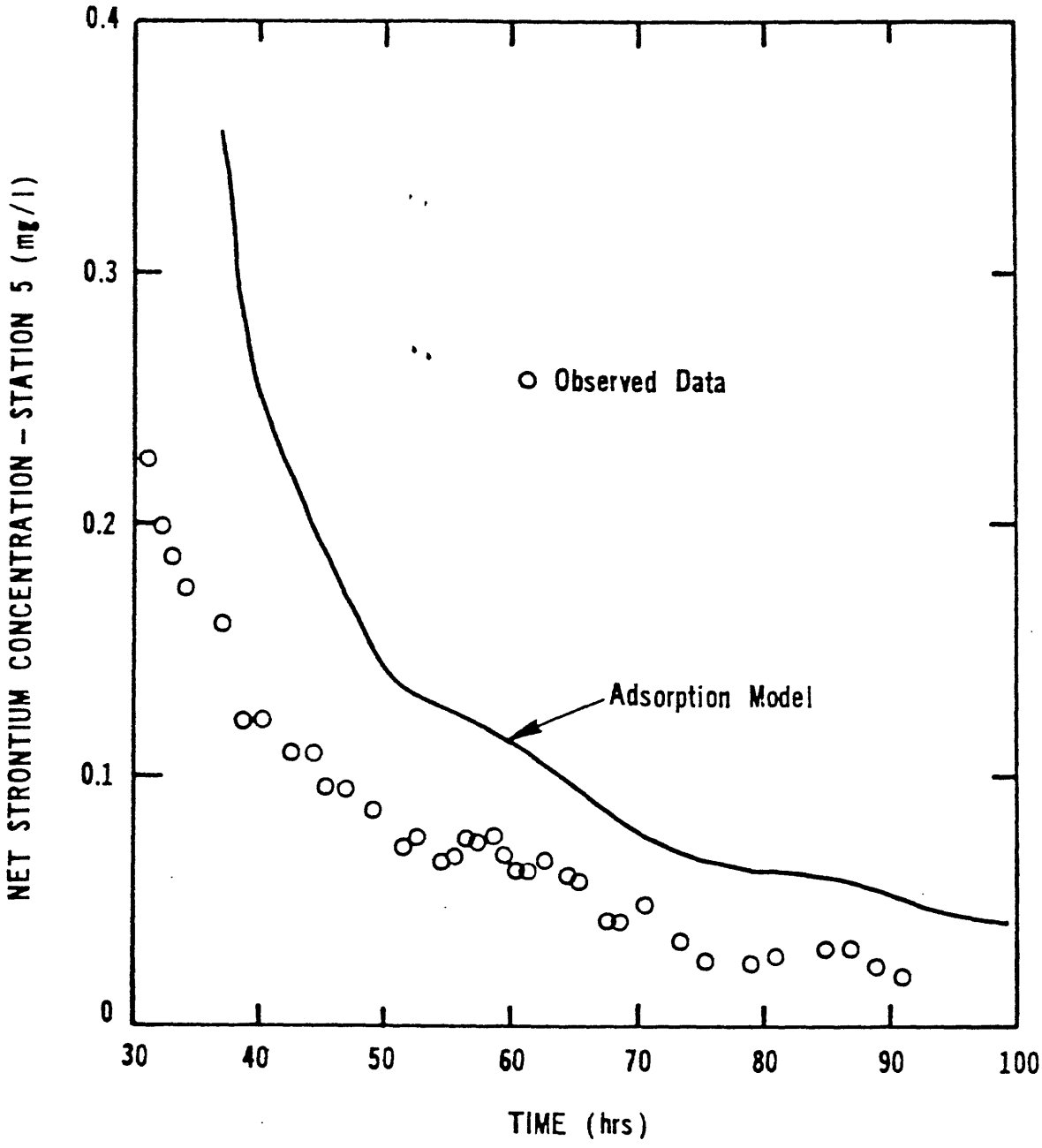

Figure 11. Comparison of net strontium concentration calculated for station 5 using the adsorption model with observed data for the period from hour 30 to hour 100.

adsorption, the strontium pulse could move only at a small fraction of the hydraulic velocity. The latter explanation, analogous to chromotographic retardation, appears more likely as there is little indication of irreversible binding of Sr in the literature or in our laboratory data.

Obviously, the adsorption model employed here requires modification if it is to accurately predict movement of adsorbed species in an environment similar to that at Uvas Creek. Addition of an irreversible bed reaction term, e.g. a first order reaction rate expression, would lower the concentrations predicted in the tail with little increase in computational difficulty. Such a model may, however, lack a physical basis. A more realistic model might be a modification of the underflow model for transport of conservative species to include adsorption. Obtaining solutions for such a model will be more difficult computationally.

SUMMARY AND CONCLUSIONS

A one-dimensional convection-dispersion transport model for conservative solutes (those not reacting in bulk solutions or with the bed) has been tested using three different models of the bed storage process. The first storage model views the bed as a well mixed compartment which exchanges material with the stream in direct proportion to the difference between stream concentration and storage compartment concentration. The second views the bed as a vertical zone into or out of which the solute may diffuse. The third assumes tht there are distinct channels within the bed through which some fraction of the streamflow passes before returning to the main channel.

The models have been tested using detailed high quality field data collected at Uvas Creek, California. Whereas all models are able to predict the experimental data with great accuracy after calibration, there are distinct differences. These differences appear to indicate that the diffusion and underflow mechanisms are both operative in Uvas Creek. However, the model employing the well mixed bed storage compartment produced adequate predictions with less computation.

A one-dimensional convective dispersion transport model for solutes which adsorb on the streambed was also developed and tested using data from Uvas Creek. This model assumes that adsorption rate is controlled by the rate of diffusion of solute into or out of the bed particles which are of uniform size and planar geometry. The model agrees reasonably well with experimental data on divalent strontium. However, the comparison shows the need for improvements in the model. The model fails to account for convection or diffusion in the bed, mechanisms which the conservative solute modeling indicates may be of importance. Accounting for these processes

would appear to be desirable although it would be difficult computationally. The model also does not account for any irreversible storage process (fixation) which may be important for some adsorbing systems.

REFERENCES CITED

Aris, R., 1957, Chemical Engineering Science, v. 6, p. 262.

Bird, R. B., Stewart, W. E. and Lightfoot, E. L., 1960, Transport Phenomena: New York, John Wiley and Sons, 780 p.

Bunzl, K., Schmidt, W. and Sansoni, B., 1976, Kinetics of ion exchange in soil organic matter. IV. Adsorption and desorption of Pb^{2+}, Cu^{2+}, Cd^{2+}, Zn^{2+} and Ca^{2+} by peat: Journal Soil Science, 27, p. 32-41.

Day, T. J., 1975, Longitudinal Dispersion in Natural Channels: Water Resources Research, v. 11, p. 909-918.

Harlemen, D.R.F., 1971, One dimensional models, in Ward, G. H., Jr. and Espey, W. H., Jr., eds., Estuarine modeling: An assessment: Tracor, Inc., Austin, Texas, p. 34-101. Available National Technical Information Service, Springfield, Va. No. PB-206807.

Hellferich, F., 1962, Ion Exchange: New York, McGraw-Hill Book Co.

Jenne, E. A., 1977, Trace element sorption by sediments and soils-sites and processes, in Symposium on molybdenum in the environment: Chapel, W. and Petersen, K., eds., New York, M. Dekker, Inc., p. 425-553.

Kennedy, V. C., 1965, Mineralogy and cation-exchange capacity of sediments from selected streams: U.S. Geological Survey Professional Paper 433-D, 28 p.

Malcolm, R. L. and Kennedy, V. C., 1970, Variation of cation exchange capacity and rate with particle size in stream sediment: Journal Water Pollution Control Federation, v. 42, p. R153-R160.

Pinder, G. F., and Gray, W. G., 1977, Finite element simulation in surface and subsurface hydrology: New York, Academic Press, 295 p.

Nordin, C. F. and Sabol, G. V., 1974, Empirical data on longitudinal

dispersion in rivers: U.S. Geological Survey Water-Resources Investigations 20-74.

Reddy, M. M. and Marinsky, J. A., 1971, Ion-exchange selectivity coefficients in the exchange of calcium, strontium, cobalt, nickel, zinc and cadmium ions with hydrogen ion in variously cross-linked polystyrene sulfonate cation exchanger at 25°C: Journal Macromolecular Science, Physics, v. B5, p. 135-158.

Reddy, M. M., Amdur, S., Marinsky, J. A., 1972, Application of thermodynamic measurements of polyelectrolyte solutions for prediction of ion-exchange selectivity: Journal American Chemical Society , v. 94, p. 4087-4093.

Shih, C. and Gloyna, E. F., 1969, Influence of sediments on transport of solutes: Journal Hydraulics Division, Proceedings American Society Civil Engineering, v. 95(HY4), p. 1347-1367.

Smith, J. M., 1970, Chemical engineering kinetics: New York, McGraw-Hill Book Company, 612 p.

Wahlberg, J. S. and Fishman, M. J., 1962, Adsorption of cesium on clay minerals: U.S. Geological Survey Bulletin 1140-A, 30 p.

Zand, S. M., Kennedy, V. C., Zellweger, G. W., and Avanzino, R. J., 1976, Solute transport and modeling of water quality in a small stream: Journal Research U.S. Geological Survey, v. 4, p. 233-240.

APPENDIX

Here we will develop exact expressions for the elements in the matrices defined by equations 29 and 30. This process may be considerably simplified if we recognize the simple nature of the basis function vector. A basis function will have non-zero values only on a single element. Therefore it is convenient to partition the system into elements with two dimensional basis vectors and property vectors and then later assemble the global matrix rank n+1 from the element matrices of rank 2. Thus we define the element basis

$$\underline{B}^e = \begin{bmatrix} \dfrac{x_2 - x}{x_2 - x_1} \\ \\ \dfrac{x - x_1}{x_2 - x_1} \end{bmatrix} = \begin{bmatrix} B_1^e \\ \\ B_2^e \end{bmatrix} \qquad \text{(A1)}$$

and we may simplify this by defining the natural coordinate on the element as

$$\xi = \frac{x - x_1}{x_2 - x_1} \qquad \text{(A2)}$$

so that

$$\underline{B}^e = \begin{bmatrix} 1 - \xi \\ \\ \xi \end{bmatrix} \qquad \text{(A3)}$$

Similarly we define element property vectors such as the concentration as

$$\underline{C}^e = \begin{bmatrix} C_1 \\ \\ C_2 \end{bmatrix} \tag{A4}$$

We may now proceed on an element by element basis to evaluate the $\underline{\underline{R}}$, $\underline{\underline{S}}$ and $\underline{T}$ of equation 30. Comparing equations 29 and 30 we see that

$$\underline{\underline{R}} = \int_0^L \underline{B}\ \underline{B}^T\ \underline{A}\ \underline{B}^T\ dx$$

$$\underline{\underline{S}} = \int_0^L \underline{B}\ \underline{B}^T \underline{Q}\ \frac{d\underline{\underline{B}}^T}{dx}\ dx \quad + \quad \int_0^L \frac{d\underline{\underline{B}}}{dx}\ \underline{B}^T\ \underline{A}\ \underline{B}^T\ \underline{D}\ \frac{d\underline{\underline{B}}^T}{dx}\ dx \tag{A5}$$

$$\underline{T} = -\int_0^L \underline{B}\ \underline{B}^T\ \underline{A}\ \underline{B}^T\ \underline{S}_b\ dx \ + \ M_{in}\ \underline{e}_1 - M_{out}\ \underline{e}_{n+1}$$

Breaking the integral for $\underline{R}$ up into integrals over the individual elements

$$\underline{\underline{R}}^e = \int_{x_i}^{x_{i+1}} \underline{B}^e\ \underline{B}^{eT}\ \underline{A}\ \underline{B}^{eT}\ dx = \int_0^1 \begin{bmatrix} 1-\xi \\ \xi \end{bmatrix} \begin{bmatrix} 1-\xi, & \xi \end{bmatrix} \begin{bmatrix} A_1 \\ A_2 \end{bmatrix} \begin{bmatrix} 1-\xi, & \xi \end{bmatrix} h_e\ d\xi$$

Where $h_e = x_{i+1} - x_1$, the length of the ith element. Performing multiplications we find

$$\underline{R}^e = h_e \int_0^1 \begin{bmatrix} (1-\xi)^2 & \xi(1-\xi) \\ \xi(1-\xi) & \xi^2 \end{bmatrix} \left((1-\xi)A_1 + \xi A_2 \right) d\xi$$

and integrating

$$\underline{\underline{R}}^e = \frac{h_e}{12} \begin{bmatrix} 3A_1+A_2 & A_1+A_2 \\ A_1+A_2 & A_1+3A_2 \end{bmatrix} = \begin{bmatrix} r_{11}^e & r_{12}^e \\ r_{21}^e & r_{22}^e \end{bmatrix} \qquad \text{(A6)}$$

We may now carry out the same operations for $\underline{\underline{S}}^e$ using the fact that

$$\frac{d\underline{B}^e}{dx} = \frac{d\underline{B}^e}{d\xi} \frac{d\xi}{dx} = \begin{bmatrix} -1 \\ 1 \end{bmatrix} \frac{1}{h_e} \qquad \text{(A7)}$$

We will simplify by evaluating the two integrals independently.

$$\int_{x_i}^{x_{i+1}} \underline{B}^e \, \underline{B}^{eT} \, \underline{Q} \, \frac{d\underline{B}^T}{dx} \, dx = \int_0^1 \begin{bmatrix} 1-\xi \\ \xi \end{bmatrix} \begin{bmatrix} 1-\xi, & \xi \end{bmatrix} \begin{bmatrix} Q_1 \\ Q_2 \end{bmatrix} \begin{bmatrix} -1, & 1 \end{bmatrix} d\xi$$

$$= \int_0^1 \begin{bmatrix} -(1-\xi) & (1-\xi) \\ -\xi & \xi \end{bmatrix} \begin{bmatrix} Q_1 (1-\xi) + Q_2 \xi \end{bmatrix} d\xi \qquad \text{(A8)}$$

$$= \frac{1}{6} \begin{bmatrix} -2Q_1 - Q_2 & 2Q_1 + Q_2 \\ -Q_1 - 2Q_2 & Q_1 + 2Q_2 \end{bmatrix}$$

and

$$\int_{x_i}^{x_{i+1}} \frac{d\underline{B}^e}{dx} \underline{B}^{eT} \underline{A} \underline{B}^{eT} \underline{D} \frac{d\underline{B}^{eT}}{dx}$$

$$= \frac{1}{h_e} \int_0^1 \begin{bmatrix} -1 \\ 1 \end{bmatrix} \left((1-\xi)A_1 + \xi A_2 \right) \left((1-\xi)D_1 + \xi D_2 \right) \begin{bmatrix} -1, 1 \end{bmatrix} d\xi$$

$$= \frac{1}{h_e} \begin{bmatrix} 1 & -1 \\ -1 & 1 \end{bmatrix} \int_0^1 (1-\xi)^2 A_1 D_1 + (1-\xi)(\xi)(A_1 D_2 + A_2 D_1$$

$$+ \xi^2 A_2 D_2 \, d\xi \qquad \text{(A9)}$$

and performing the matrix multiplication

$$\underline{T}^e = \frac{h_e}{12} \begin{bmatrix} (3A_1+A_2)S_{b1} + (A_1+A_2)S_{b2} \\ (A_1+A_2)S_{b1} + (A_1+3A_2)S_{b2} \end{bmatrix} \tag{A10}$$

Now we may globally assemble the $\underline{\underline{R}}^e$ which overlap on the diagonal to form $\underline{\underline{R}}$

$$\underline{\underline{R}} = \begin{bmatrix} r_{11}^1 & r_{12}^1 & 0 & 0 & & & \\ r_{21}^1 & (r_{22}^1+r_{11}^2) & r_{12}^2 & 0 & & & \\ 0 & r_{21}^2 & (r_{22}^2+r_{11}^3) & r_{21}^3 & & & \\ 0 & 0 & r_{21}^3 & (r_{22}^3+r_{11}^4) & & & \\ & & & & & & 0 \\ & & & & & & r_{12}^n \\ & & & & 0 & r_{21}^n & r_{22}^n \end{bmatrix}$$

$$= \frac{1}{6h_e} \begin{bmatrix} 1 & -1 \\ -1 & 1 \end{bmatrix} (2A_1D_1 + A_1D_2 + A_2D_1 + 2A_2D_2)$$

Finally,

$$\underline{T}^e = \int_{x_i}^{x_{i+1}} \underline{B}^e \, \underline{B}^{eT} \, \underline{A} \, \underline{B}^{eT} \, \underline{S}_b \, dx = \underline{\underline{R}}^e \, \underline{S}_b^e$$

or, from (A6)

$$\underline{T}^e = \frac{h_e}{12} \begin{bmatrix} 3A_1+A_2 & A_1+A_2 \\ A_1+A_2 & A_1+3A_2 \end{bmatrix} \begin{bmatrix} S_{b1} \\ S_{b2} \end{bmatrix}$$

$$= h_e \int_0^1 \begin{bmatrix} 1-\xi \\ \xi \end{bmatrix} \left\{ (1-\xi)^2 A_1 S_{b1} + \xi(1-\xi) A_1 S_{b2} + \xi(1-\xi) A_2 S_{b1} + \xi^2 A_2 S_{b2} \right\} d\xi$$

$$= \frac{h_e}{12} \begin{bmatrix} 3A_1S_{b1} + A_1S_{b2} + A_2S_{b1} + A_2S_{b2} \\ A_1S_{b1} + A_1S_{b2} + A_2S_{b1} + 3A_2S_{b2} \end{bmatrix}$$

which we may rewrite as

$$R = \begin{bmatrix} r_{11} & r_{12} & 0 & 0 & 0 & & \\ r_{21} & r_{22} & r_{23} & 0 & 0 & & \\ 0 & r_{32} & r_{33} & r_{34} & 0 & & \\ 0 & 0 & \ddots & \ddots & \ddots & \ddots & 0 \\ & & & \ddots & \ddots & \ddots & r_{n,n+1} \\ & & & 0 & 0 & r_{n+1,n} & r_{n+1,n+1} \end{bmatrix} \qquad \text{(A11)}$$

where

$$r_{ii} = \frac{h_{i-1}}{12}(A_{i-1} + 3A_i) + \frac{h_i}{12}(3A_i + A_{i+1}) \quad 2 \leq i \leq n$$

$$r_{11} = \frac{h_1}{12}(3A_1 + A_2)$$

$$r_{n+1,n+1} = \frac{h_n}{12}(A_n + 3A_{n+1})$$

$$r_{i+1,i} = r_{i,i+1} = \frac{h_i}{12} (A_i + A_{i+1})$$

Combining equations A9 and A10, we may globally assemble the elements of $\underline{\underline{S}}^e$ to form $\underline{\underline{S}}$

$$\underline{\underline{S}} = \begin{bmatrix} s_{11} & s_{12} & 0 & 0 & 0 & & 0 \\ s_{21} & s_{22} & s_{23} & 0 & 0 & & \\ 0 & s_{32} & s_{33} & s_{34} & 0 & & \\ 0 & 0 & \ddots & \ddots & \ddots & \ddots & \\ & & & & & & s_{n,n+1} \\ & & & & & s_{n+1,n} & s_{n+1,n+1} \end{bmatrix} \qquad \text{(A12)}$$

$$s_{i,i} = \frac{1}{6} (Q_{i-1} - Q_{i+1}) + \frac{1}{6h_{i-1}} (2A_{i-1}D_{i-1} + A_{i-1}D_i + A_iD_{i-1} + 2A_iD_i)$$

$$+ \frac{1}{6h_i} (2A_iD_i + A_iD_{i+1} + A_{i+1}D_i + 2A_{i+1}D_{i+1}) \qquad 2 \leq i \leq n$$

$$s_{1,1} = \frac{1}{6} (-2Q_1 - Q_2) + \frac{1}{6h_1} (2A_1D_1 + A_1D_2 + A_2D_1 + 2A_2D_2)$$